https://doi.org/10.5194/essd-2026-379
Preprint. Discussion started: 22 July 2026

Open Access Earth System Science Data Discussions

Long-term multi-site eddy-covariance observations of carbon, water, and energy fluxes in West Africa

Luitpold Hingerl[inst1,inst3], Samuel Guug[inst2], Jan Bliefernicht[inst1], Hawwa Kadum[inst3], Souleymane Sy[inst1], Windmanagda Sawadogo[inst2], Emmanuel Quansah[inst4], Francis E. Oussou[inst1,inst2,inst5], Leonard Amekudzi[inst4], Seyni Salack[inst2], Belko Abdul-Aziz Diallo[inst2], Michael Ayamba[inst2], Emmanuel Ramde[inst4], Rainer Steinbrecher[inst3], Frank Neidl[inst3], and Harald Kunstmann[inst1,inst3]

[inst1]Institute of Geography, University of Augsburg, Augsburg, Germany
[inst2]WASCAL Competence Center, West African Science Service Center on Climate Change and Adapted Land Use, Ouagadougou, Burkina Faso
[inst3]Institute for Meteorology and Climate Research (IMKIFU), Karlsruhe Institute of Technology, Garmisch-Partenkirchen, Germany
[inst4]Department of Meteorology and Climate Science, Kwame Nkrumah University of Science and Technology, Kumasi, Ghana
[inst5]Laboratoire d'Hydrologie Appliquée, Institut National de l'Eau (INE), Université d'Abomey-Calavi, Cotonou, Benin

Correspondence: Luitpold Hingerl (luitpold.hingerl@kit.edu)

Abstract. Long-term ecosystem–atmosphere flux measurements are crucial for understanding land–atmosphere interactions, ecosystem functioning, and climate variability. In West Africa's Sudanian savanna, such data are limited despite rapid land use change and high climate sensitivity. We address this by providing a harmonized, multi-site eddy covariance dataset of carbon, water, and energy fluxes from six savanna ecosystems in Burkina Faso and Ghana.

The dataset provides half-hourly and daily turbulent CO_2, latent and sensible heat fluxes, net radiation, meteorological variables, and, where available, soil moisture and soil temperature. Measurements span the period 2013–2025 across contrasting land-use types ranging from forest savanna to cropland and degraded grassland. All data were processed with a uniform EddyPro-based workflow and further post-processed to ensure physical plausibility, temporal consistency, and harmonized variable definitions. Quality flags accompany all turbulent fluxes for user-defined filtering.

Archived in the PANGAEA repository and openly available (DOI: https://doi.org/10.1594/PANGAEA.994143), the dataset's temporal continuity, explicit quality information, and multi-year coverage support diverse applications, including land surface and Earth system model evaluation, land–atmosphere coupling studies, satellite and machine-learning product validation, and analyses of seasonal to interannual variability and hydroclimatic extremes. These long-term, quality-controlled flux observations from a climate-sensitive, underrepresented region provide a key resource for advancing process understanding and model development in West African savannas.

1 Introduction

The West African Sudanian Savanna is undergoing rapid environmental change, primarily driven by population growth, agricultural expansion and urbanization (Waller et al., 2007; Neupane and Kumar, 2015; Flörke et al., 2018; Xue, 2017; Potapov

https://doi.org/10.5194/essd-2026-379
Preprint. Discussion started: 22 July 2026

et al., 2022; Bliefernicht et al., 2018). These anthropogenic pressures substantially modify land surface characteristics and ecosystem structure, thereby altering land–atmosphere interactions, surface energy partitioning, and the exchange of carbon dioxide and water vapor with the atmosphere (Snyder et al., 2004; Boone et al., 2016; Sy et al., 2017; Mortey et al., 2023). This is particularly relevant in West Africa, which has been identified as a global hotspot of land–atmosphere coupling (Koster et al., 2004, 2006). In this region, soil-moisture variability exerts a particularly strong control on surface energy fluxes and precipitation variability, rendering the climate system especially sensitive to land use change and climate variability and making West Africa a priority region for process-based observations.

Eddy covariance (EC) techniques provide direct, continuous measurements of ecosystem-scale exchanges of carbon, water, and energy and have become a cornerstone of terrestrial ecosystem research and global carbon cycle assessments (Verhoef et al., 1996; Hutley et al., 2005; Yu et al., 2019). In West Africa, most EC studies have been restricted to short observation periods of one to three years and a small number of sites, which hampers robust assessments of interannual variability, long-term trends, and ecosystem responses to hydroclimatic extremes (Ago et al., 2015; Aryee et al., 2020).

Existing EC studies in Burkina Faso and Benin have demonstrated pronounced diurnal, seasonal, and interannual variability in carbon dioxide, water vapor, and energy fluxes, largely controlled by rainfall seasonality and soil moisture availability (Brümmer et al., 2008; Ago et al., 2016; Mamadou et al., 2016). Clear differences between ecosystem types have been reported, with higher productivity and sustained seasonal carbon uptake in forested and near-natural savanna systems compared to cropland and degraded grassland (Ago et al., 2015, 2016; Ceperley et al., 2017; Quansah et al., 2015). In contrast, degraded savanna and woodland ecosystems often approach carbon neutrality or function as a net source under persistent water limitation and grazing pressure, underscoring the importance of land management and conservation for maintaining regional carbon sinks (Ago et al., 2015; Quansah et al., 2015; Berger et al., 2019). Longer-term flux observations from cultivated and mixed savanna systems further highlight strong management effects and large year-to-year variability in carbon balances (Ago et al., 2014; Koukoui et al., 2025; Mamadou et al., 2025).

Beyond ecosystem responses, methodological studies in West African savannas have emphasized persistent challenges associated with EC measurements, including incomplete energy balance closure, heterogeneous flux footprints, and site-specific turbulence regimes (Bagayoko et al., 2006; Nadolski et al., 2024). Such challenges are particularly relevant in savanna environments, where strong seasonal changes in surface roughness, atmospheric stability, and land use heterogeneity can violate classical similarity assumptions and complicate flux interpretation (Hutley et al., 2005). Nevertheless, long-term EC datasets are indispensable for quantifying ecosystem "memory effects", assessing responses to droughts and anomalous rainfall events, and developing and testing robust quality control and gap filling approaches (Gao et al., 2023; Abdaki et al., 2025). Recent syntheses further indicate a decline in carbon sequestration strength in semi-arid African savannas over the past decade, attributed to increasing atmospheric dryness, highlighting the urgency of sustained observations in the region (Wieckowski et al., 2024).

To address this, coordinated observational efforts such as the West African Science Service Center on Climate Change and Adapted Land Use (WASCAL) have established a hydrometeorological observatory with long-term EC measurements across contrasting land use types in the Sudanian savanna of Burkina Faso and Ghana (Bliefernicht et al., 2013; Quansah et al., 2015; Bliefernicht et al., 2018; Berger et al., 2019; Guug et al., 2025; Hingerl et al., 2025; Sy et al., 2026). While early field

https://doi.org/10.5194/essd-2026-379
Preprint. Discussion started: 22 July 2026

campaigns in West Africa (e.g., SEBEX, HAPEX-Sahel, NIMEX) provided valuable process level insights, most observations were campaign-based, temporally limited, or are no longer operational. An exception is the AMMA-CATCH observatory, which integrates long term mesoscale hydrological and land-surface observations across several eco-climatic zones in West Africa (Benin, Niger, Mali). Established to assess the impacts of climate and land use transitions on the regional water cycle and critical zone dynamics, AMMA-CATCH has provided valuable multi-year datasets across a number of sites, supporting studies on vegetation–hydrology feedbacks and hydro-climatic variability (Lebel et al., 2009; Lohou et al., 2014; Galle et al., 2018).

However, despite these important efforts, long term observations of turbulent carbon, water, and energy exchange remain very limited in semi-arid West Africa. In particular, continuous multi-year eddy-covariance measurements are still exceptionally scarce, and openly accessible datasets processed according to harmonized FLUXNET standards are virtually absent for the region. Existing records are typically restricted to a few years, a small number of sites, or earlier observation periods, such that long term flux measurements reflecting recent climatic conditions (post-2020) and ongoing land use change are still largely lacking. The WASCAL EC network therefore represents one of the very few sustained and standardized micrometeorological observatories in the Sudanian Savanna, explicitly designed to resolve land use gradients under comparable climatic forcing. These sites provide a unique framework for investigating land–atmosphere exchange processes along land use and management gradients under a shared climatic regime, while also enabling multi-year analyses that capture interannual variability, extreme hydroclimatic events, and legacy effects of land management.

Here, we present a harmonized and quality-controlled eddy-covariance dataset from six contrasting Sudanian savanna ecosystems in Burkina Faso and Ghana, covering two main measurement periods. To our knowledge, this dataset constitutes one of the most comprehensive multi-year EC records currently available for semi-arid Africa. It combines long-term flux observations across a representative land use gradient and spans both pre- and post-2015 climatic conditions, thereby capturing recent environmental change. In addition to making the dataset publicly available, we provide a consistent multi-site analysis that extends beyond previous studies (Berger et al., 2019; Guug et al., 2025; Hingerl et al., 2025) (include Quansah/Nadolski). This integrated perspective allows us to quantify land use-related differences in seasonal and diurnal dynamics, turbulence and stability fingerprints and energy balance characteristics across ecosystems.

The measurement campaign was structured into two primary phases, followed by a consolidation phase. The first phase (2013–2016) involved three EC towers (Nazinga - protected forest, Kayoro - cropland and Sumbrungu - degraded grassland), one of which (Sumbrungu) had to be decommissioned in 2016 due to vandalism (Bliefernicht et al., 2013, 2018). This decommissioned station was subsequently reinstalled under comparable land use conditions (Gorigo) and resumed operation in 2017. After the initial main measurement period, a consolidation phase followed, during which the three stations Nazinga, Kayoro and Gorigo largely continued operating. The second measurement period (2022–2025) includes four EC stations, of which two were newly installed (Janga - rainfed rice field, Mole - managed forest site), one continues operating since the first measurement period (Kayoro - cropland) and one was relocated during the consolidation phase (Gorigo - semi-degraded grassland). The dataset includes half hourly and daily aggregates of CO_2, H_2O, and energy fluxes, ancillary meteorological variables, and energy balance closure diagnostics, processed following FLUXNET community standards. By making these data openly

https://doi.org/10.5194/essd-2026-379
Preprint. Discussion started: 22 July 2026

Open Access Earth System Science Data Discussions

available via the PANGAEA repository, we aim to provide the research community with a rare multi-year observational basis for studies of land–atmosphere coupling, model and reanalysis evaluation, satellite validation, and assessments of land use and climate impacts on ecosystem functioning in one of the world's most climate-sensitive savanna regions.

2 Sites and instrumentation

2.1 Site description

The study sites are grouped according to their dominant land use and management characteristics, including forest, cropland, and grassland ecosystems.

2.1.1 Forest sites

The Nazinga site is located within the Nazinga Game Ranch, in the core protection zone of the park (Bliefernicht et al., 2018). It represents a Sudanian savanna ecosystem in a largely undisturbed state, without active agricultural management. The site is referred to as near-natural, since a complete absence of anthropogenic influence on the vegetation cannot be guaranteed, given the region's historically high population density. Owing to its protected status within a national park, it serves as a reference site for minimally disturbed land–atmosphere exchange processes. The vegetation consists of a heterogeneous mixture of grasses, shrubs, and trees (Berger et al., 2019). During the rainy season, grass heights can reach up to 2.5 m (Table 1). Trees in the surrounding area typically range from 4 to 5 m in height, with the tallest individuals attaining 8 to 10 m (Bliefernicht et al., 2018). The soil texture is comparable to that of the degraded grassland but exhibits a higher clay fraction. Moreover, the soil organic carbon content is the highest among all sites, reaching 3.3% (Table 1).

The Mole site is the second EC station installed during the second phase of the measurement campaign in May 2023 and is located within Mole National Park in northern Ghana. Vegetation structure and species composition are comparable to the Nazinga site, consisting of a mosaic of grasses, shrubs, and scattered trees. In contrast to the Nazinga site, the Mole Forest Reserve is subject to active management interventions, specifically the implementation of controlled burns. As part of the CONCERT-driven extension of the WASCAL observatory, the Mole station is equipped with an upgraded sensor setup to ensure high-quality, continuous measurements under protected conditions.

2.1.2 Cropland and rainfed rice field

The Kayoro site is located in a sparsely populated area. It represents a cropland ecosystem that is alternately used for rain-fed cultivation and left fallow. During fallow periods, grass may reach heights of up to 1 m (Table 1). When the land is under cultivation the area surrounding the EC tower is largely covered by groundnut crops, which attain an average height of about 30 cm. The soil texture is comparable to that of the other sites but differs in chemical composition, with a lower organic carbon content of 0.62 % in the topsoil (Table 1). The terrain at the Kayoro site is flat, consistent with the topography observed at the other EC stations.

https://doi.org/10.5194/essd-2026-379
Preprint. Discussion started: 22 July 2026

The Janga site was installed during the second phase of the measurement campaign in June 2022 in an agricultural field primarily used for rainfed rice cultivation. During the plantation and early growth period, the field is temporarily flooded following rainfall events, resulting in persistently high soil water contents. Rice plants reach maximum heights of approximately 1 m shortly before harvest. Outside the growing season, the field is typically left fallow, with sparse residual vegetation or bare soil prevailing during the dry season. It should be noted that rice cultivation was conducted only during the first year of measurements (2023). In the subsequent years, rice cultivation was hindered by recurring dry periods, leading to unsuccessful planting attempts, and the field was eventually left fallow and became predominantly colonized by spontaneous grass vegetation. The site was established to represent an intensively managed cropland system and to contrast near-natural savanna ecosystems within the WASCAL observatory network.

2.1.3 Grassland sites

The Sumbrungu site is located northwest of Bolgatanga in northern Ghana. It represents a strongly degraded savanna area that is subject to intensive land use and grazing pressure. At present, crop cultivation occurs only in lower slope positions within the surrounding landscape (Berger et al., 2019). The area within approximately 200 m of the EC tower is predominantly used year round as rangeland for livestock (Berger et al., 2019), with an estimated stocking density of 6–8 animals per hectare (Quansah et al., 2015). As a consequence, the grass height rarely exceeds 10 cm, even during the rainy season. The immediate surroundings of the tower are sparsely vegetated with individual trees and shrubs, averaging around 5 m in height, spaced roughly 50 m apart (Bliefernicht et al., 2018), and together covering about 3% of the site area. A photograph of the EC station and its characteristic vegetation during the wet-to-dry transition period is shown in Figure 1. The soil at the Sumbrungu site is classified as loamy sand with a high fraction of coarse material down to approximately 50 cm depth (Bliefernicht et al., 2018). Despite its degraded condition, the topsoil still contains a relatively high amount of organic carbon (1.6%; Table 1).

Following severe vandalism at the Sumbrungu site in 2016, which caused an interruption of measurements, the EC station was reinstalled under comparable land use and environmental conditions slightly further north and is referred to as Gorigo (Bliefernicht et al., 2022). The relocation aimed to ensure the continuation of long-term observations of a degraded savanna ecosystem while maintaining consistency with the original site characteristics. Land use at Gorigo is primarily characterized by intensive grazing and sparse vegetation cover, resembling conditions at the former Sumbrungu site, although the area is less degraded. While the site is mainly used for livestock grazing, some patches surrounding the EC station were occasionally cultivated with maize during the 2018 and 2019 measurement period. Thereafter, the area reverted exclusively to grazing, as the degraded soils were unable to sustain sufficiently high crop yields. Minor differences in measurement configuration, including a slightly higher sensor installation height, were introduced during reinstallation and are documented in detail in the instrumentation section. These changes affect the effective footprint scale and warrant a reclassification of Gorigo from a degraded savanna comparable to the former Sumbrungu site to a semi-degraded grassland site within the WASCAL observatory network. This revised classification reflects its lower degree of degradation, which enabled the temporary cultivation of maize during the years 2018 and 2019.

https://doi.org/10.5194/essd-2026-379
Preprint. Discussion started: 22 July 2026

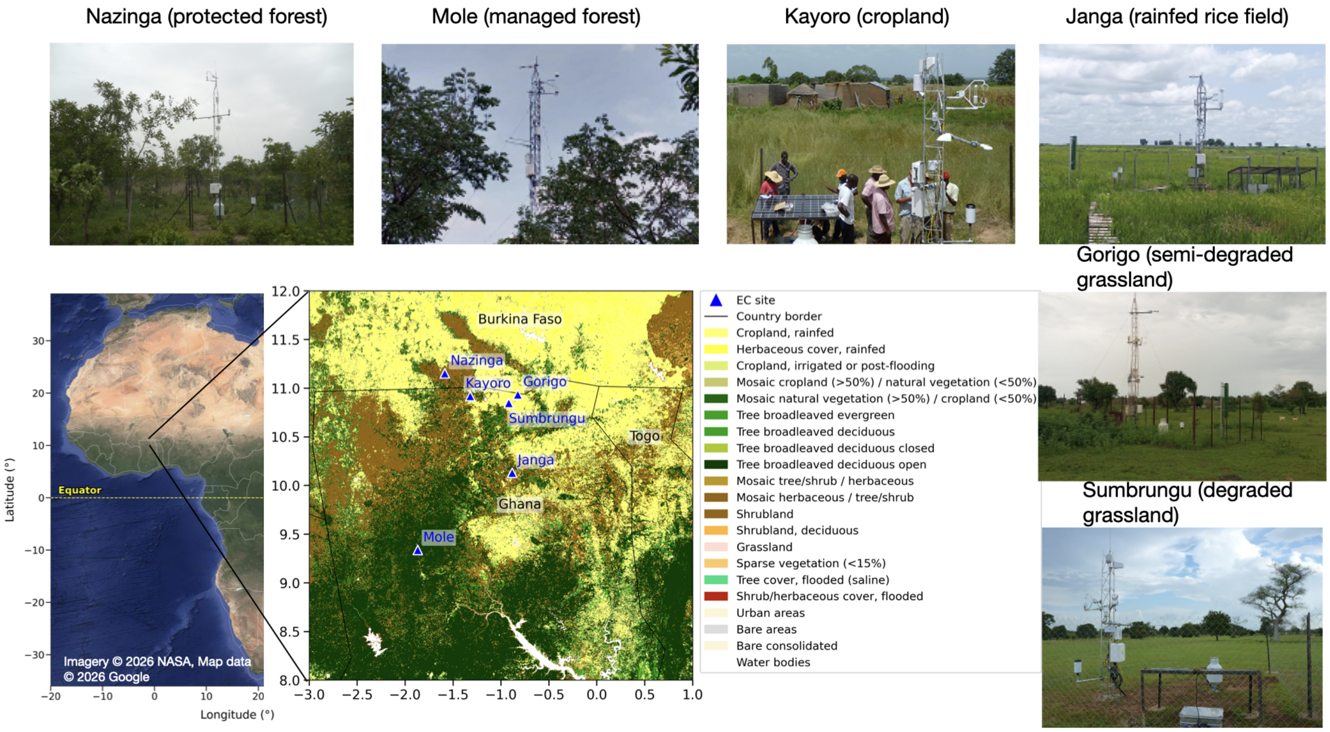

Figure 1. The location of the selected EC stations. Background: Copernicus Climate Change Service Land Cover v2.1.1 (300 m resolution, year 2022; Copernicus Climate Change Service, 2023). The EC stations belong to the mesoscale observatory operated by WASCAL and its partner institutions in this region since 2013

2.2 Site instrumentation

The stations deployed during the first phase of the measurement campaign (Nazinga, Kayoro, Sumbrungu), as well as Gorigo, which replaced Sumbrungu following the relocation during the consolidation phase in 2017, are all equipped with an identical set of sensors. To quantify the turbulent exchange of energy and mass, three dimensional wind components were recorded with a sonic anemometer (CSAT3, Campbell Scientific), and an open-path infrared gas analyzer (LI-7500A, LI-COR) measured H_2O and CO_2 concentrations and air pressure. Air temperature and relative humidity was obtained from a co-located temperature and humidity probe (HMP155A, Campbell) which is protected by a ventilated radiation shield. The signals of these sensors were sampled at 20 Hz. Alongside the high frequency measurements, additional variables were recorded at 5 minute intervals. For energy balance closure assessment, continuous measurements of incoming and outgoing short and longwave radiation were obtained using a CNR4 net radiometer (Kipp & Zonen; Blonquist Jr et al. (2009)). Precipitation is measured with three independent sensors, each operating on a different measurement principle: a tipping bucket (52203, R.M. Young), a weighing gauge (Pluvio2, Ott) and a disdrometer as component of a compact weather station (WXT 520, Vaisala). The use of three independent precipitation sensors allows cross validation and improves the robustness of rainfall measurements, particularly

https://doi.org/10.5194/essd-2026-379
Preprint. Discussion started: 22 July 2026

Table 1. Basic climate, land use and soil characteristics of the selected savanna sites (protected forest, cropland, rainfed rice field, semi-degraded and degraded grassland) (Bliefernicht et al., 2018; Berger et al., 2019).

Characteristic	**Nazinga**	**Kayoro**	**Sumbrungu**	**Gorigo**	**Janga**	**Mole**
Land use	Protected forest	Cropland	Degr. grassland	Semi-degr. grassland	Rainfed rice field	Managed forest
Land use intensity	Very low	High	High	High	High	Very low
Max. grass height [m]	2.5	1	0.1	0.1	1	3
Mean tree height [m]	4.5	5	5	5	0	8
Latitude, °N	11.1556	10.91810	10.84660	10.936	10.130	9.336
Longitude, °W	-1.58570	-1.32900	-0.91700	-0.824	-0.884	-1.869
Altitude [m a.s.l.]	293	292	200	217	118	159
Mean annual precipitation [mm]	994	960	978	826	707	972
Mean annual temperature [°C]	28.6	29.2	28.3	27.9	29.4	29.3
Soil organic carbon content [mass-%]	3.30	0.62	1.60	0.50	0.62	1.62

during short and intense convective events. In addition, the measurement system includes a set of soil sensors. Three self-calibrating soil heat flux plates (HFP01SC, Hukseflux) are installed at a depth of 8 cm, while soil moisture is monitored at 3 cm using CS616 reflectometers (Campbell Scientific). Soil temperature is measured at 3, 10, and 35 cm depths with a TCAV averaging thermocouple probe (Campbell Scientific). Data were recorded using CR3000 and CR1000 data loggers (Campbell Scientific).

The two sites Janga and Mole, which were installed during the second phase of the measurement campaign, feature a setup similar to the earlier stations but include several additional sensors and use different data loggers. Turbulent flux measurements were complemented by a laser spectroscopy gas analyzer (LI-7700, LI-COR) for the determination of CH_4 concentrations. Although CH_4 concentrations were measured at Janga and Mole, this data is not included in the present data release and are reserved for future dedicated analyses. Additionally the concentrations of CO_2 and H_2O and the three dimensional wind field are measured with an IRGASON, which is a combination of a sonic anemometer and an open-path infrared gas analyzer (CSAT3A and EC150, Campbell Scientific). Soil moisture is now monitored at depths of 3, 10, and 35 cm, thereby providing a vertical profile that is consistent with the corresponding soil temperature measurements. Data acquisition is performed using a CR6 data logger (Campbell Scientific). Sensor installation heights vary between sites to account for differences in vegetation structure and land use and are documented in detail in Table 2.

https://doi.org/10.5194/essd-2026-379
Preprint. Discussion started: 22 July 2026

Table 2. Overview of measured variables, sampling frequency, temporal resolution, and sensor heights for all EC stations.

Variable	Stat.	Temp. res.	Sumbrungu		Kayoro		Nazinga		Gorigo		Janga		Mole	
			Freq.	Height	Freq.	Height	Freq.	Height	Freq.	Height	Freq.	Height	Freq.	Height
Eddy-covariance wind & scalars														
Zonal wind component ($m\,s^{-1}$)	mean	30 min	20 Hz	2.65	20 Hz	3.15	20 Hz	7.19	20 Hz	4.3	20 Hz	3.4	10 Hz	12
Meridional wind component ($m\,s^{-1}$)	mean	30 min	20 Hz	2.65	20 Hz	3.15	20 Hz	7.19	20 Hz	4.3	20 Hz	3.4	10 Hz	12
Vertical wind component ($m\,s^{-1}$)	mean	30 min	20 Hz	2.65	20 Hz	3.15	20 Hz	7.19	20 Hz	4.3	20 Hz	3.4	10 Hz	12
Sonic air temperature (°C)	mean	30 min	20 Hz	2.65	20 Hz	3.15	20 Hz	7.19	20 Hz	4.3	20 Hz	3.4	10 Hz	12
Water vapour conc. ($g\,m^{-3}$)	mean	30 min	20 Hz	2.65	20 Hz	3.15	20 Hz	7.19	20 Hz	4.3	20 Hz	3.4	10 Hz	12
CO_2 conc. ($mg\,m^{-3}$)	mean	30 min	20 Hz	2.65	20 Hz	3.15	20 Hz	7.19	20 Hz	4.3	20 Hz	3.4	10 Hz	12
Radiation components														
SW↓, LW↓, SW↑, LW↑ ($W\,m^{-2}$)	mean	5 min	1/15 Hz	2.00	1/15 Hz	2.50	1/15 Hz	5.30	1/15 Hz	6.9	1/15 Hz	5.4	1/15 Hz	12
Auxiliary meteorology														
Air temperature (°C)	mean	5 min	20 Hz	2.65	20 Hz	3.15	20 Hz	7.19	20 Hz	4.3	20 Hz	3.4	10 Hz	12
Relative humidity (%)	mean	5 min	20 Hz	2.65	20 Hz	3.15	20 Hz	7.19	20 Hz	4.3	20 Hz	3.4	10 Hz	12
Precipitation amount (mm)	sum	5 min	1/15 Hz	1.00	1/15 Hz	1.0	1/15 Hz	1.0	1/15 Hz	1.0	1/15 Hz	1.0	1/15 Hz	1.0
Soil profile and surface fluxes														
Soil temperature (°C) at 3 cm	mean	5 min	1/15 Hz	0.03	1/15 Hz	0.03	1/15 Hz	0.03	1/15 Hz	0.03	1/15 Hz	0.03	1/15 Hz	0.03
Soil temperature (°C) at 10 cm	mean	5 min	1/15 Hz	0.1	1/15 Hz	0.1	1/15 Hz	0.1	1/15 Hz	0.1	1/15 Hz	0.1	1/15 Hz	0.1
Soil temperature (°C) at 35 cm	mean	5 min	1/15 Hz	0.35	1/15 Hz	0.35	1/15 Hz	0.35	1/15 Hz	0.35	1/15 Hz	0.35	1/15 Hz	0.35
Volumetric water content (%) at 3 cm	mean	5 min	1/15 Hz	0.03	1/15 Hz	0.03	1/15 Hz	0.03	1/15 Hz	0.03	1/15 Hz	0.03	1/15 Hz	0.03
Volumetric water content (%) at 10 cm	mean	5 min	-	-	-	-	-	-	-	-	1/15 Hz	0.1	1/15 Hz	0.1
Volumetric water content (%) at 35 cm	mean	5 min	-	-	-	-	-	-	-	-	1/15 Hz	0.35	1/15 Hz	0.35
Ground heat flux ($W\,m^{-2}$)	mean	5 min	1/15 Hz	0.08	1/15 Hz	0.08	1/15 Hz	0.08	-	-	1/15 Hz	0.08	1/15 Hz	0.08

3 Processing and quality control of EC data

3.1 EddyPro processing

The high frequency EC data (20 Hz) was processed using EddyPro v7.0.9 (LI-COR Biosciences, 2021). All processing steps are documented in the station specific EddyPro project files and follow a consistent workflow among sites. Raw turbulence data was subjected to automated plausibility tests, despiking, and statistical screening following Vickers and Mahrt (1997) as implemented in EddyPro. Absolute limits, signal range checks, skewness and kurtosis tests, amplitude resolution tests, and drop-out detection were enabled to remove physically and electronically implausible values. Detrending was performed by block averaging over the flux averaging interval. The coordinate rotation was applied using the double rotation method (Kaimal and Finnigan, 1994).

Two sensor configurations were operated across the stations. At Mole and Janga, fluxes were measured using integrated IRGASON system, in which the sonic anemometer and the open-path gas analyzer share the same measurement volume,

https://doi.org/10.5194/essd-2026-379
Preprint. Discussion started: 22 July 2026

thereby minimizing sensor separation effects. At the remaining stations, a separated configuration consisting of a CSAT3 sonic anemometer and a LI-7500A open-path infrared gas analyzer was used. For these stations, additional high-frequency spectral attenuation caused by sensor separation was explicitly corrected. Spectral corrections were applied to account for high and low frequency attenuation following the transfer function approach of Moore (1986). EddyPro's spectral analysis routines were used to derive correction factors based on measured cospectra and theoretical transfer functions. Corrections included path averaging, dynamic sensor response, block averaging losses, zero-order hold effects, and electronic filtering. For the separated CSAT3 + LI-7500A configuration, sensor separation effects were additionally considered. Fluxes were corrected for density fluctuations using the Webb–Pearman–Leuning (WPL) correction (Webb et al., 1980; Schotanus et al., 1983; Liebethal and Foken, 2003; Jentzsch et al., 2021). The evaluation of turbulence quality followed the stationarity test of Foken and Wichura (1996) and the integral turbulence characteristics framework described in Mauder et al. (2013). The quality flags used follow the Spoleto agreement (Mauder et al., 2013) and are assigned to all half hourly fluxes, indicating the reliability of the data (0 = high, 1 = moderate, 2 = low quality). Fluxes flagged as "2" were excluded from the data set (see Table 3 for the proportion of retained data). Flux footprint diagnostics were calculated using the analytical model of Kormann and Meixner (2001) for quality control and interpretation. The output variables were standardized according to FLUXNET conventions to ensure compatibility with the community data formats and facilitate reuse of the data set.

3.2 Quality control and post-processing

This section describes additional quality control and post-processing steps applied after EddyPro processing to ensure physical plausibility, temporal consistency, and comparability of the final half hourly data products. Physically plausible ranges were defined, and observations falling outside these bounds were excluded and recoded as missing values. Quality filtering based on the quality flags computed with EddyPro was not applied; however, the corresponding flag columns were retained and included in the dataset. For subsequent analyses, it is strongly recommended to utilize only data associated with a quality flag $QC \leq 1$. Data with QC = 2 have been excluded from the aggregated data products as well as from the technical validation of this data set presented in the following chapters. To ensure methodological consistency and facilitate comparability across observations, all data were resampled and aggregated to a uniform temporal resolution of 30 minutes. The specific aggregation procedure was selected according to the type of variable. State and flux variables were processed by computing arithmetic means over each 30-minute interval, whereas precipitation was aggregated by summation over the corresponding periods. Note that no gap filling has been performed; instead, missing observations have been explicitly annotated as missing values. For further information on temporal continuity and the structure of data gaps, we refer the reader to the chapter on Data availability. This facilitates the versatile applicability of the data set across a variety of gap-filling methodologies. Additionally, the post-processed data have been standardized with respect to sign conventions, units, and variable nomenclature. As a result of the applied post-processing procedure, the data product represents a quality controlled and harmonized collection of half hourly EC measurements. All filtering and aggregation techniques employed are documented in a comprehensive and fully transparent manner. In addition to the general quality control procedures, a site-specific quality flag was introduced for the Kayoro station to account for a structural change in the footprint area. A school building constructed in October 2016 is located within a

https://doi.org/10.5194/essd-2026-379
Preprint. Discussion started: 22 July 2026

Table 3. Quality control (QC) statistics for sensible heat flux (H), latent heat flux (LE), and CO_2 fluxes across all EC stations. The table reports the total number of half hourly records (n), as well as the number and percentage of records with acceptable quality ($QC \leq 1$) and very good quality ($QC = 0$).

			QC ≤ 1		QC = 0	
Station	Variable	Total n	n	%	n	%
Nazinga	H	92 762	85 173	91.8	70 047	75.5
Nazinga	LE	78 396	70 187	89.5	54 973	70.1
Nazinga	CO_2	83 311	75 641	90.8	59 976	72.0
Kayoro	H	154 828	139 952	90.4	100 767	65.1
Kayoro	LE	145 125	130 687	90.1	81 407	56.1
Kayoro	CO_2	145 115	134 764	92.9	93 251	64.3
Sumbrungu	H	43 144	38 666	89.6	27 219	63.1
Sumbrungu	LE	40 961	35 566	86.8	22 687	55.4
Sumbrungu	CO_2	42 221	38 082	90.2	26 515	62.8
Gorigo	H	78 760	71 946	91.3	56 271	71.4
Gorigo	LE	74 977	70 492	94.0	51 016	68.0
Gorigo	CO_2	74 832	70 772	94.6	52 697	70.4
Janga	H	41 770	36 443	87.2	24 426	58.5
Janga	LE	33 392	28 435	85.2	17 413	52.1
Janga	CO_2	33 440	29 198	87.3	18 961	56.7
Mole	H	33 852	29 689	87.7	20 279	59.9
Mole	LE	31 259	27 159	86.9	17 941	57.4
Mole	CO_2	33 687	29 327	87.1	19 487	57.8

sector of the dominant flux footprint. Therefore, all observations from October 2016 onwards with wind directions between 196° and 228° were flagged as potentially affected (QC_wind_sector_kayoro = 1), while all other observations were marked as unaffected (flag = 0). Rather than removing these data, the flag is provided to allow users to apply their own filtering strategies depending on the specific application.

3.3 Site specific data coverage

The data availability varies between the six sites and reflects the step wise extension of the WASCAL obeservatory as described in chapter 2.2 and the site specific events related to installation, relocation, technical issues and calibration of sensors (Figure 2). The heatmap shows the percentage of data availability per month for the entire measurement period for six central variables

https://doi.org/10.5194/essd-2026-379
Preprint. Discussion started: 22 July 2026

Open Access Earth System Science Data Discussions

Table 4. Overview of variables provided in the half-hourly (30 min) and daily aggregated TSV data products. Column names follow the PANGAEA requirement that full parameter names and units are provided in the first header row.

Column header in TSV files	**Description / additional information**
Event and spatiotemporal reference	
Event	Station/event label
Elevation [m a.s.l.]	Elevation above sea level; constant per site
Date/Time [UTC]	Start of averaging period; ISO 8601, UTC
Eddy-covariance fluxes	
Latent heat flux [W m^{-2}]	30 min mean turbulent flux
Latent heat flux quality flag [-]	QC flag: 0 = high, 1 = moderate, 2 = low quality
Sensible heat flux [W m^{-2}]	30 min mean turbulent flux
Sensible heat flux quality flag [-]	QC flag: 0 = high, 1 = moderate, 2 = low quality
Net ecosystem CO_2 exchange [μmol CO_2 m^{-2} s^{-1}]	Negative values indicate net ecosystem CO_2 uptake
CO_2 flux quality flag [-]	QC flag: 0 = high, 1 = moderate, 2 = low quality
Momentum flux [kg m^{-1} s^{-2}]	Turbulent shear stress
Momentum flux quality flag [-]	QC flag: 0 = high, 1 = moderate, 2 = low quality
Friction velocity [m s^{-1}]	Derived from momentum flux
Stability parameter z/L [-]	Dimensionless Monin–Obukhov stability parameter
Monin–Obukhov length [m]	Derived stability length scale
Radiation components	
Incoming shortwave radiation [W m^{-2}]	30 min mean
Outgoing shortwave radiation [W m^{-2}]	30 min mean reflected shortwave radiation
Incoming longwave radiation [W m^{-2}]	30 min mean
Outgoing longwave radiation [W m^{-2}]	30 min mean
Net radiation [W m^{-2}]	Net radiative flux
Water balance variables	
Precipitation [mm]	Sum over 30 min interval
Evapotranspiration [mm]	Derived from latent heat flux
Meteorological variables	
Atmospheric pressure [kPa]	30 min mean
Air temperature [$^\circ$C]	30 min mean
Relative humidity [%]	30 min mean
Vapour pressure deficit [hPa]	Derived from air temperature and humidity
Wind direction [degree]	30 min mean; meteorological convention
Wind speed [m s^{-1}]	30 min mean
Soil measurements	
Soil heat flux [W m^{-2}]	Measured at 8 cm depth
Volumetric soil water content at 3 cm depth [%]	30 min mean
Volumetric soil water content at 10 cm depth [%]	30 min mean; available for Janga and Mole
Volumetric soil water content at 35 cm depth [%]	30 min mean; available for Janga and Mole
Soil temperature at 3 cm depth [$^\circ$C]	30 min mean
Soil temperature at 10 cm depth [$^\circ$C]	30 min mean
Soil temperature at 35 cm depth [$^\circ$C]	30 min mean
Site-specific quality flags	
Kayoro wind sector quality flag [-]	1 = potentially affected by school building footprint sector; 0 = unaffected

https://doi.org/10.5194/essd-2026-379
Preprint. Discussion started: 22 July 2026

Open Access Earth System Science Data Discussions

(Precipitaion (P), net radiation (R_n), latent heat flux (LE), sensible heat flux (H), CO_2 flux (CO_2) and volumetric soil water content (θ). It should be noted that quality filtering of the turbulent fluxes based on the aforementioned quality flags has not been applied to the data set; instead, the corresponding flags are provided in a separate column. The data have, however, been screened using physically plausible thresholds, and all observations exceeding these limits have been removed accordingly.

In addition to the monthly coverage shown in Figure 2, the temporal continuity of the turbulent flux time series was assessed using gap-length statistics (Figure B1). The gap-length distributions indicate that missing data predominantly occur as very short gaps at all sites. For LE, H, and CO_2 the median gap length is 0.5 hours, corresponding to a single 30-minute averaging interval. Longer gaps, ranging from several hours to multiple days, occur with substantially lower frequency and are primarily associated with maintenance periods, technical issues, or phases excluded by quality control. Overall, the dominance of short gaps demonstrates a high degree of temporal continuity of the EC time series.

Nazinga, Kayoro, and Gorigo provide the longest time series within the WASCAL observatory, extending back to its early phase in 2013. These sites offer high multi-year coverage of energy and CO_2 fluxes, spanning 2013–2022 for Nazinga, 2013–2025 for Kayoro, and 2017–2024 for Gorigo, thereby underlining their particular value for climatological and long-term trend analyses (Figure 2). Short time gaps are mainly caused by instrumental failures, maintenance or rigorous quality filtering during strong precipitation events. The initiation of measurements at the Gorigo site in 2017 results from the aforementioned resumption of monitoring activities under land-use conditions comparable to those at the Sumbrungu site and represents the continuation of observations of the degraded savanna land-use type. The Janga and Mole sites were commissioned during the second phase of the measurement campaign, resulting in comparatively shorter, yet internally consistent, periods of data availability. The heatmap (Figure 2) shows that both sites exhibit a high degree of data availability after deployment indicating a successful integration of the EC stations into the existing network.

3.4 Variable specific data availability and quality assessment

The turbulent flux variables LE, H, and CO_2 as well as radiation measurements exhibit consistently high data coverage across all sites. Measurements of soil heat fluxes are available for all stations except the site Gorigo, whereas soil moisture profiles are only available for the more recently established sites, Janga and Mole. Regarding the precipitation measurements, we selected the most complete time series from a single sensor at each station, which may differ between stations. The specific sensor used for the respective precipitation measurements is documented in the accompanying variable description files. For an overview of all available measured variables including units, temporal resolution, sampling frequency and measurement height please refer to Table 2. Overall the heatmap in Figure 2 reveals a high data availability for the central flux quantities across all sites. The displayed differences in temporal coverage are consistent with the site specific history and the respective installation dates and don't constitute a limitation of data quality. The integration of long-term reference sites with newly established monitoring locations facilitates climatological long-term analyses and enables the systematic investigation of current land use and management effects.

https://doi.org/10.5194/essd-2026-379
Preprint. Discussion started: 22 July 2026

Figure 2. Monthly data availability (%) for the main variables (P, R_n, LE, H, CO_2, and θ) across all six EC stations. Each row corresponds to a station–variable combination, and each column represents a month. Data coverage is shown prior to QC filtering. Abbreviations: n.a. = not accessible; n.p. = data available but not yet processed.

4 Technical validation

All validation metrics in this section were computed over the site-specific observation periods shown in Figure 2.

4.1 Energy balance closure

In Figure 3 the closure of the energy balance (EBC) is shown for five of the available stations as the slope of the linear regression line and as the cumulative closure ratio of the energy balance, calculated as $\mathrm{EBC_{cum}} = \sum(H+LE)\,/\,\sum(R_n-G)$. In addition, the coefficient of determination (R^2) of the linear regression is shown as a measure of the goodness of fit. The EBC for the Gorigo station cannot be calculated because no valid soil heat flux measurements are available. In general, the EBC indicates a

https://doi.org/10.5194/essd-2026-379
Preprint. Discussion started: 22 July 2026

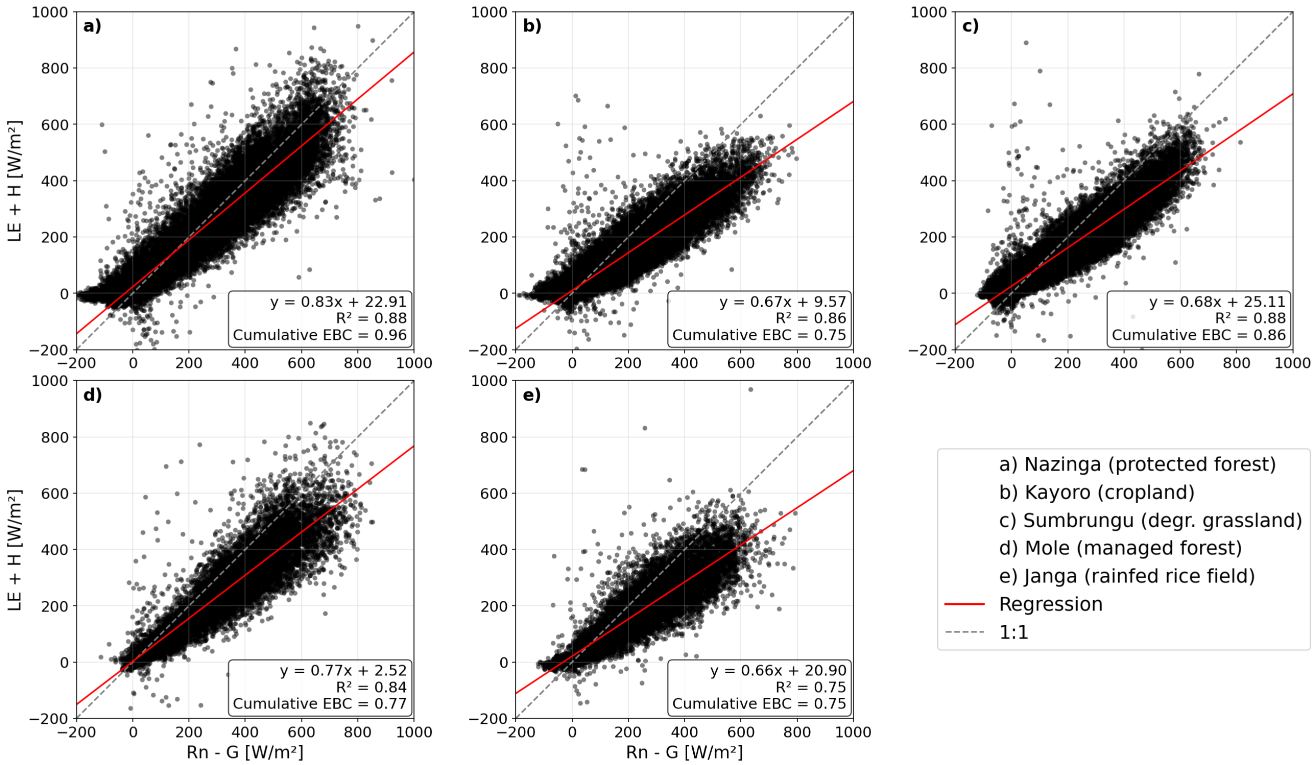

Figure 3. Surface energy balance closure and R^2 derived from time-integrated incoming and outgoing energy fluxes at multiple stations.

consistent relationship between turbulent fluxes (LE + H) and available energy (R_n - G) across sites, with closure ratios ranging between 0.67 and 0.89, corresponding to an unclosed fraction of approximately 10–30 % of the available energy. Differences between the sites reflect site specific properties like surface heterogeneity, vegetation structure and soil properties. The values of R^2 demonstrate a strong linear correspondence between turbulent fluxes and the available energy, thus supporting an overall internal consistency of the measured fluxes. Lower closure ratios and/or R^2 values may be attributed to unaccounted energy terms such as horizontal advection, heat storage, or non-turbulent transport processes that are not captured by the EC method.

4.2 Turbulence regime and stability

To assess the quality and usability of the EC measurements, the prevailing turbulence regimes characterized by the friction velocity u_* and atmospheric stability conditions described by the stability parameter $(z-d)/L$ were analyzed for all sites, separately for daytime ($SW_{in} > 10$ W m^{-2}) and nighttime conditions (Figure 4). This distinction is particularly important for the interpretation of CO_2 fluxes, as low turbulence conditions during stable boundary layers at night can lead to decoupling of the atmosphere from the surface. As a consequence storage effects and advective CO_2 transport (e.g. drainage flows) can result in non-turbulent exchange processes that are not fully captured by the EC system and may lead to a substantial underestimation

https://doi.org/10.5194/essd-2026-379
Preprint. Discussion started: 22 July 2026

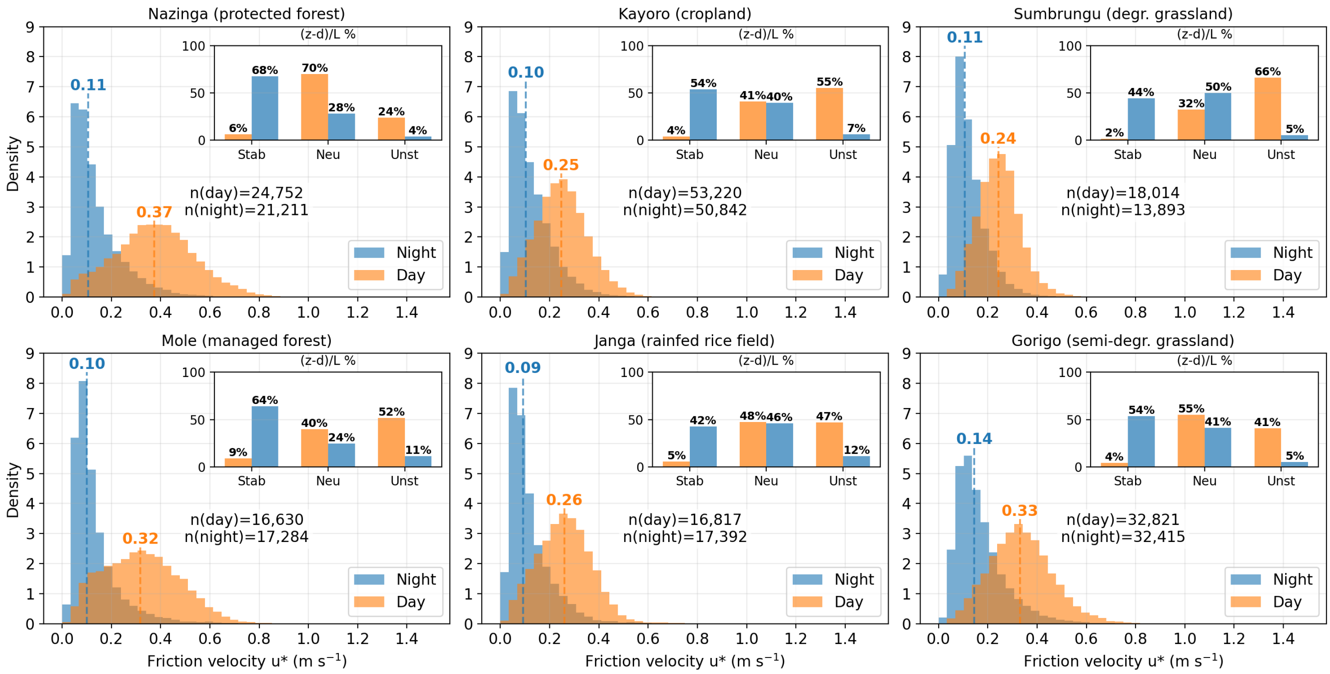

Figure 4. Turbulence and stability fingerprints of the eddy-covariance measurements at the six study sites. Shown are distributions of friction velocity (u_*) separated into daytime (incoming shortwave radiation > 10 W m^{-2}) and nighttime conditions, with dashed lines indicating median values. The daytime u_* distributions are shown transparently, allowing the nighttime distributions to remain visible where both overlap. Insets summarize the relative occurrence of atmospheric stability classes based on the stability parameter $(z-d)/L$, classified as stable ($(z-d)/L > 0.1$), near-neutral ($-0.1 \leq (z-d)/L \leq 0.1$), and unstable ($(z-d)/L < -0.1$), shown separately for day and night. Numbers denote the percentage of time spent in each stability class. The Figure highlights site-specific differences in turbulence regimes and the frequent occurrence of weakly turbulent, stable conditions, particularly during nighttime.

of ecosystem respiration (Mauder et al., 2024; Wanner et al., 2024; Butterworth et al., 2024). The density distribution of u_* in Figure 4 shows distinct patterns for day- and nighttime periods at all sites. During the day high values are clearly dominant indicating strong mixing of the boundary layer while at night less turbulent conditions prevail. Station specific differences in median u_* values reflect variations in surface roughness, vegetation structure and land use across the sites. A common feature of the near-natural sites (Nazinga and Mole) is that their daytime u_* distributions span a relatively wide range with less pronounced peaks, indicating a more evenly distributed turbulence spectrum compared to the other sites. This behavior is consistent with their higher surface roughness, which enhances shear stress and facilitates the generation of eddies over a wider range of intensities. An exception of the general pattern is the Gorigo site, which exhibits a comparatively wide range of daytime u_* distribution with a median value of 0.33, although it being classified as semi-degraded grassland, similar to Sumbrungu. This effect may be attributed to the substantially higher measurement height in Gorigo compared to Sumbrungu (see Table 2) which increases the effective footprint scale and enhances the contribution of trees and shrubs to mechanically

https://doi.org/10.5194/essd-2026-379
Preprint. Discussion started: 22 July 2026

generated turbulence. In addition, the larger number of available observations compared to the forest sites and thus a more even u_* distribution across the spectrum may contribute to this apparent similarity. These results indicate that besides land use and vegetation structure, measurement configuration also affects the turbulence characteristics.

The frequency distribution of the stability parameter $(z-d)/L$ reveals stable regimes clearly dominate at night while the daytime is characterized by neutral and unstable stratification. The two cropland sites Kayoro and Janga exhibit very similar stability distributions during both daytime and nighttime, with neutral regimes occurring at comparable frequencies of approximately 40-48 $\%$ in both periods. With respect to the turbulence and stability footprint, these two sites show the highest degree of similarity within one of the three land use classes presented in this study.

Across the near-natural sites, the stability distributions converge primarily during nighttime, when stable stratification accounts for more than 60 $\%$ of the observations. This apparent similarity, however, masks pronounced differences in the underlying turbulence regimes during daytime conditions. Although both Nazinga and Mole are classified as near-natural savanna sites, their turbulence and stability fingerprints reveal important contrasts. At Nazinga, the dense and spatially homogeneous savanna vegetation promotes locally generated turbulence and results in a comparatively well-organized stability distribution that largely conforms to Monin–Obukhov similarity theory (MOST) expectations. In contrast, the Mole site is characterized by pronounced horizontal heterogeneity caused by fire-affected patches within the flux footprint. These patches introduce strong contrasts in surface roughness and sensible heat flux, leading to advectively influenced and non-local turbulence generation. As a consequence, turbulence statistics at Mole deviate more strongly from classical MOST scaling despite the same land use classification.

Despite their similar grassland character, Sumbrungu and Gorigo differ markedly in their daytime stability class distributions, although Gorigo is classified as semi-degraded grassland and Sumbrungu as degraded grassland. Gorigo exhibits a comparatively higher occurrence of near-neutral and only weakly unstable conditions, whereas Sumbrungu is more frequently characterized by pronounced unstable stratification. Consistent with this contrast, Gorigo also shows a broader daytime u_* distribution, while the more strongly unstable conditions at Sumbrungu are associated with a comparatively narrower and more concentrated range of u_* values. This difference is in line with the contrasting measurement configurations and roughness length distributions discussed previously. The higher measurement height at Gorigo increases the effective footprint scale and amplifies the influence of trees and shrubs on mechanically generated turbulence, thereby enhancing shear-driven mixing and shifting the stability regime towards near-neutral conditions. In contrast, the lower measurement height at Sumbrungu results in a smaller, more surface-confined footprint, where buoyancy-driven turbulence dominates during daytime, leading to a higher prevalence of unstable conditions. These results indicate that differences in measurement configuration within the degraded savanna class can systematically modulate the partitioning between shear- and buoyancy-driven turbulence and consequently the observed stability class distributions.

4.3 Footprint representativeness

Figure 5 shows the mean footprints for two representative months of the rainy and dry season, namely July 2023 and January 2024, at the EC sites Mole, Janga, and Gorigo. These months were selected because they correspond to the climatological peak

https://doi.org/10.5194/essd-2026-379
Preprint. Discussion started: 22 July 2026

of the rainy season and the core of the dry season across the study region, thereby providing the clearest contrast in atmospheric stability, prevailing wind direction, and footprint extent. In addition, both months were characterized by comparatively complete and continuous data availability at all three sites. A detailed footprint analysis for the remaining sites of the WASCAL network (Nazinga, Kayoro and Sumbrungu) was previously presented by Hingerl et al. (2025). That study showed that the effective source area of the EC measurements typically extends up to about 150 m upwind of the tower and exhibits a clear seasonal rotation associated with the West African Monsoon circulation. Despite differences in land-surface heterogeneity among sites, the footprints remain largely confined to the characteristic land use types surrounding the towers, indicating a generally high representativeness of the measured fluxes.

The footprints at the three sites analysed here also exhibit a clear seasonal modulation caused by the shift in prevailing wind direction from south-west during the rainy season to north-east during the dry season. However, the magnitude of this directional modulation differs between sites. It is most pronounced at Gorigo, the northernmost of the three shown in Figure 1, somewhat weaker at Janga, and least pronounced at Mole, the southernmost site. This pattern suggests that the seasonal footprint modulation decreases toward lower latitudes along the transect.

The footprints at the Mole site cover in both seasons areas with differing burning histories. Particularly during the rainy season, burned surface patches characterized by reduced aerodynamic roughness and enhanced sensible heat fluxes are incorporated into the measurement footprint. This heterogeneity constitutes a potential source of advective contributions to the observed turbulent fluxes. The Janga site is characterized by comparatively uniformly shaped footprints, particularly pronounced during the rainy season. The predominantly agricultural and structurally homogeneous surroundings promote a locally governed generation of turbulence. At the Gorigo site, the footprint exhibits a pronounced dependence on the prevailing wind direction, particularly during the dry season, resulting in a more elongated and directionally oriented footprint shape compared to the other sites. Due to the greater effective measurement height relative to Sumbrungu (see Table 2), more distant structural elements such as trees and shrubs may contribute to the footprint, thereby increasing the potential influence of mechanically generated turbulence. In general the footprints indicate, that differences in land use, surface heterogeneity and measurement configuration have a significant effect on the source area of the measured fluxes. Despite seasonal shifts in wind direction, the mean footprints remain spatially coherent and confined to the characteristic land use types of each site, indicating a high degree of representativeness of the measured fluxes across seasons.

4.4 Event based consistency checks

To evaluate the internal consistency of the measured water balance variables, we conduct an event-based analysis at a sub-daily temporal scale. Thus, we focus on isolated precipitation events occurring during the transitional season or the onset of the rainy season, when the soil profile is not yet fully saturated, and examine the temporal dynamics of soil moisture and ET in response to these events. These event-based consistency checks enable a qualitative evaluation of the physical plausibility of the data and of the response of the soil–plant–atmosphere system to water inputs. Initially, discrete precipitation events were identified, and associated temporal analysis windows were defined to encompass antecedent and subsequent periods spanning from 48 hours prior to 72 hours following the onset of each event. The temporal response to these events consistently exhibits

https://doi.org/10.5194/essd-2026-379
Preprint. Discussion started: 22 July 2026

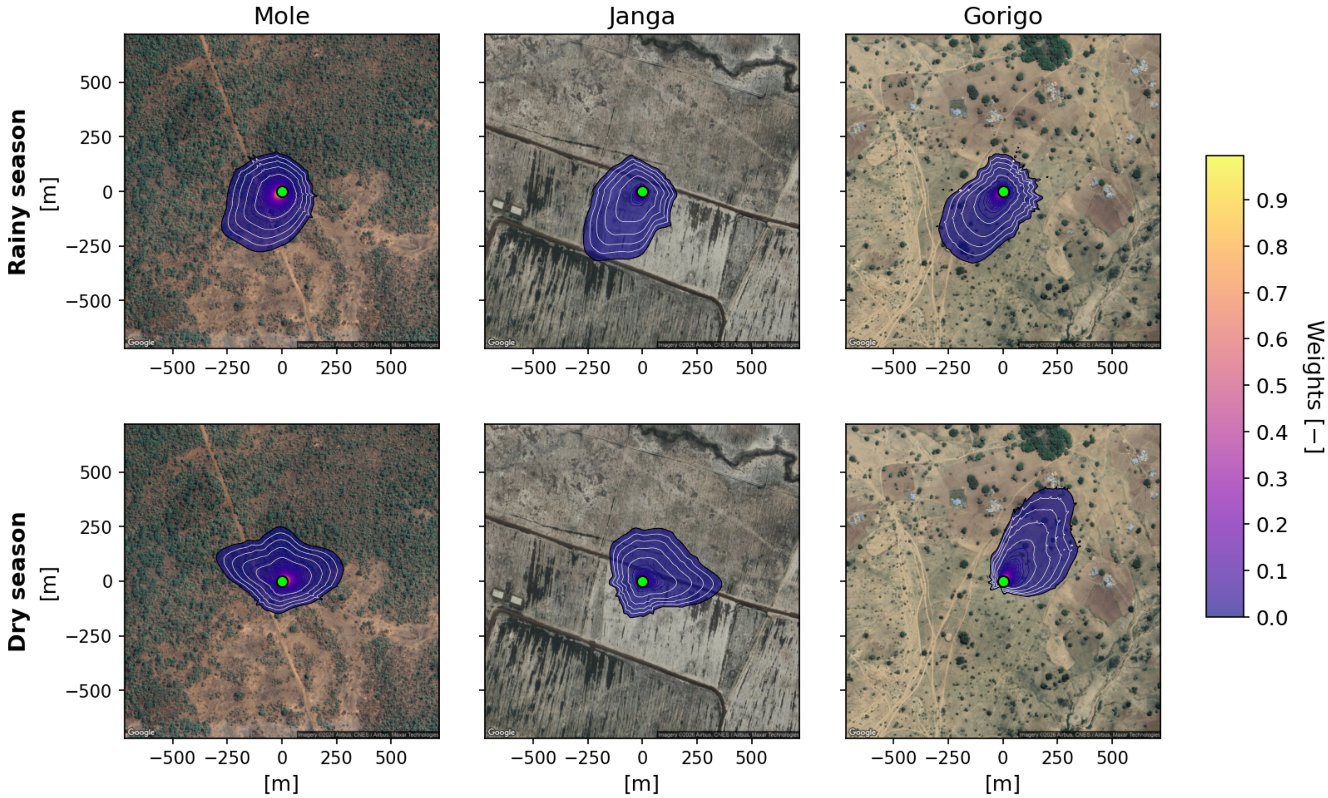

Figure 5. Mean flux footprints for the three EC stations Gorigo, Mole and Janga for two representative months: July 2023 (rainy season) and January 2024 (dry season). Background satellite imagery is provided by Google; imagery © 2026 Airbus, CNES / Airbus, Maxar Technologies.

an immediate increase in θ, within the shallow soil layers ($3\,\mathrm{cm}$) at all sites. In the deeper soil layers, a delayed and attenuated response to the water input is observed. ET shows an equally coherent response to the precipitation events with an immediate increase on the next day. Regarding the dynamics of both ET and θ, we observe distinct site-specific differences that reflect the respective characteristics of the three land use types. The forest sites Nazinga and Mole exhibit comparatively high daily pre-event amplitudes of ET and, consequently, a smaller relative increase in ET following precipitation events. A relatively high vegetation density, in combination with an increased proportion of trees and shrubs possessing deep root systems, exerts a stabilizing effect on ET and dampens its immediate response to precipitation events. The reduction in ET at the cropland and rainfed rice field sites (Kayoro and Janga) and degraded and semi-degraded grassland (Sumbrungu and Gorigo), corresponds closely to the temporal decline in water content within the upper soil layer after the precipitation event, whereas this coupling is less pronounced at the forest sites. With respect to the volumetric water content in the deeper soil layers (10–35 cm), which is currently recorded only at the most recently installed stations Mole and Janga, markedly different dynamics are observed.

https://doi.org/10.5194/essd-2026-379
Preprint. Discussion started: 22 July 2026

Open Access Earth System Science Data Discussions

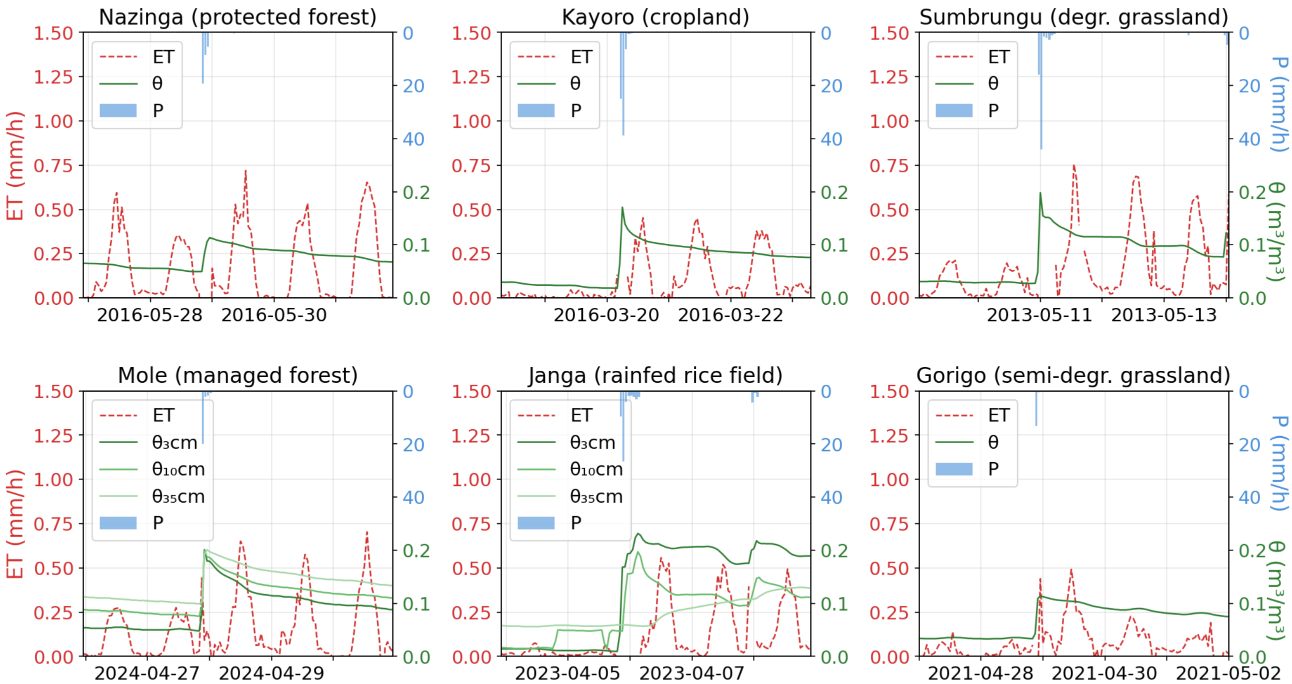

Figure 6. Event-scale water balance forcing vs. storage response for the six EC stations. Precipitation (bars) and evapotranspiration (lines) are shown together with the soil volumetric water content (θ; lines). Stations with soil moisture profiles include θ at 3, 10, and 35 cm, while stations with only shallow sensors show θ at 3 cm.

At the Mole site, all monitored layers respond to the precipitation event almost immediately and in a relatively uniform manner. This behavior suggests a high soil porosity, most likely associated with a dense root system in the vegetated surface layer. In contrast, the Janga site exhibits a strongly dampened response, characterized by an increasing response gradient with increasing depth. This pattern is likely attributable to lower overall soil porosity and a higher proportion of clay in the upper soil horizons, resulting from tillage practices. Furthermore, the absence of vegetation and associated root networks during this pre-sowing period may additionally reduce soil porosity and thus contribute to the attenuated hydrological response. In summary, event-based consistency checks confirm a physically plausible coupling between precipitation, soil moisture, and evapotranspiration at all sites. The site-specific response patterns reflect expected differences in land use and soil properties, indicating a consistent representation of water balance processes at event scale.

4.5 Climatological and diurnal patterns

Figure 7 displays the seasonal climatology of CO_2 exchange between ecosystem and the atmosphere and the running sum of precipitation averaged for each day of year (DOY) over all available data for the six study sites. All sites exhibit a pronounced seasonal pattern, characterized by declining CO_2 fluxes with increasing cumulative precipitation, eventually reaching negative

https://doi.org/10.5194/essd-2026-379
Preprint. Discussion started: 22 July 2026

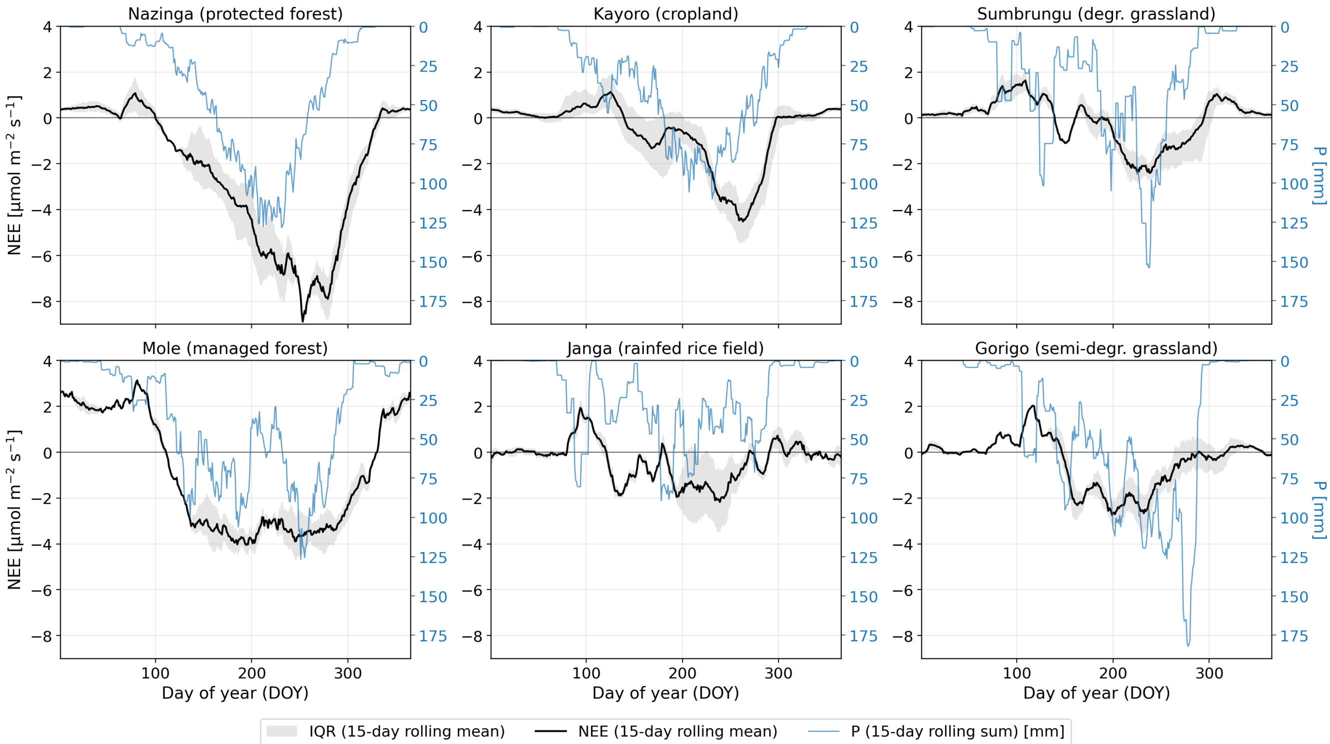

Figure 7. Seasonal climatology of ecosystem–atmosphere CO_2 exchange derived from quality-controlled eddy-covariance measurements (QC $\leq$ 1) at the six study sites. Shown are multi-year seasonal cycles of daily turbulent CO_2 fluxes aggregated by day of year (DOY). Solid lines indicate the smoothed mean flux, while the shaded envelope represents the interquartile range (IQR; 25th–75th percentile). half hourly CO_2 fluxes were first aggregated to daily means, grouped by DOY across all available years, and subsequently smoothed using a 15-day rolling mean with circular boundary conditions. Negative flux values denote net ecosystem CO_2 uptake. Note that the storage term is not included; therefore, the fluxes approximate net ecosystem exchange (NEE), particularly during daytime, but may underestimate nighttime respiration under stable atmospheric conditions. For context, the secondary axis shows the smoothed 15-day running sum of precipitation. The Figure illustrates site-specific differences in the timing, magnitude, and duration of seasonal carbon uptake and highlights the strong coupling between CO_2 exchange and seasonal rainfall dynamics in Sudanian savanna ecosystems.

values indicative of net ecosystem CO_2 uptake. The observed seasonal coupling between cumulative precipitation and CO_2 exchange closely matches the patterns reported by Quansah et al. (2015) for Nazinga, Kayoro, and Sumbrungu, who demonstrated a strong control of rainfall seasonality on the timing and magnitude of net ecosystem CO_2 uptake. The climatological perspective adopted here confirms that these site-specific patterns persist across multiple years and are not driven by individual seasons or anomalous conditions.

When comparing Nazinga and Mole, notable differences emerge in the seasonal pattern of CO_2 exchange, despite both sites being classified as forest savanna. Although Nazinga exhibits a moderately elevated CO_2 signal during the dry season, the corresponding signal at Mole is substantially more pronounced. With respect to carbon uptake, we observe at Mole a peak that

https://doi.org/10.5194/essd-2026-379
Preprint. Discussion started: 22 July 2026

is of lower amplitude but broader temporal extent during the rainy season compared to that recorded at the Nazinga site. This discrepancy is likely attributable to site-specific surface heterogeneity, as the footprint analysis indicates that extensive portions of the Mole site footprint intersect fire-affected patches. Within these patches, vegetation structure and surface roughness can be substantially altered, thereby modulating the climatological CO_2 exchange signal. However, the prescribed burns conducted during the dry season are themselves likely to contribute substantially to the pronounced source signal observed at this site. The broader period of peak carbon uptake at Mole follows the bimodal precipitation pattern, which is likely associated with the seasonal northward and southward passage of the Intertropical Convergence Zone over the site, thereby prolonging the wet season and extending the period of active vegetation growth. In contrast, the reference site Nazinga exhibits the highest CO_2 uptake of all sites during the rainy season, reaching peak values of approximately $-8\ \mu mol\ m^{-2}\ s^{-1}$, nearly twice those observed at the managed forest site Mole. This stronger uptake likely reflects the more vigorous and uninterrupted vegetation growth in the protected savanna at Nazinga, whereas carbon assimilation at Mole is constrained by forest management and the more heterogeneous vegetation structure.

The cropland and rainfed rice field sites Kayoro and Janga exhibit smaller and shorter seasonal patterns of carbon uptake compared to the forest sites. At both sites the onset of the rainy season initially triggers a transition from net CO_2 release to uptake, but the subsequent seasonal evolution differs markedly. At Kayoro, CO_2 uptake develops gradually after the onset of the rainy season and reaches a relatively pronounced minimum after the peak of the rainy season, indicating a coherent period of vegetation growth and carbon uptake. The broad interquartile range, however, suggests that this pattern can be interrupted by periods of carbon release in some years, likely reflecting year to year differences in land management practices. In contrast, Janga shows a much more irregular and fragmented seasonal pattern. Periods of net CO_2 uptake are shorter and interrupted by repeated returns towards near-neutral or even positive fluxes. The strongest uptake occurs earlier and is less persistent than at Kayoro. This behaviour is likely related to the specific management and phenology of the rice field at Janga, where flooding, transplanting, and harvest cycles can strongly modify the timing and magnitude of ecosystem respiration and assimilation. The comparatively weak net uptake at Janga further suggests that periods of enhanced respiration partly offset the photosynthetic signal.

Similar irregularity in the seasonal pattern of CO_2 exchange exhibit the degraded and semi-degraded grassland sites Sumbrungu and Gorigo. Both systems function as net CO_2 sources during the dry season and transition to a period of moderate net CO_2 uptake following the onset of the rainy season; however, this uptake is considerably weaker than that observed at the forest reference sites. Similar to the rainfed rice field site Janga the degraded grassland sites exhibit strong short term fluctuations and a relatively fragmented signal, including a short release period well after the onset of the rains at Sumbrungu. This suggests that, although both sites are characterized by degraded vegetation cover and a constrained capacity for carbon uptake, the land-atmosphere exchanges at Sumbrungu exhibit greater temporal variability, potentially reflecting heightened grazing pressure or other differences in land management practices. These site-specific differences in seasonal CO_2 exchange are likewise reflected in the mean diurnal cycles of NEE (Appendix Figure C1), with the forest sites exhibiting the strongest daytime CO_2 uptake and the largest diurnal amplitudes. Similar variability has also been reported by Quansah et al. (2015), who attributed year

https://doi.org/10.5194/essd-2026-379
Preprint. Discussion started: 22 July 2026

Open Access Earth System Science Data Discussions

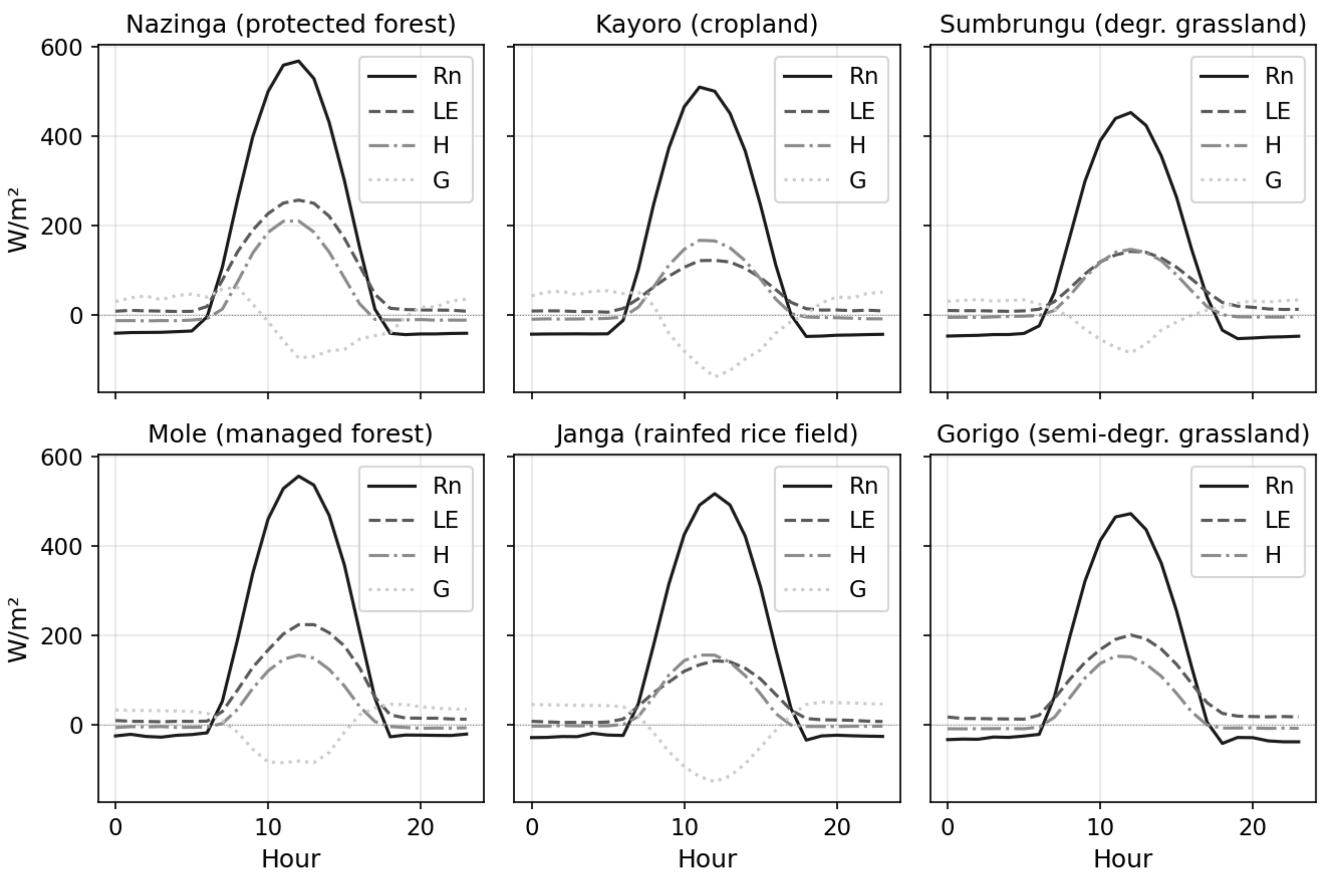

Figure 8. Mean diurnal cycles of the energy balance components across all EC stations.

430 to year variations in net ecosystem CO_2 uptake primarily to variation in the temporal distribution of precipitation events and precipitation amount.

To complement the climatological patterns of CO_2 exchange, Figure 8 shows the mean diurnal cycles of the energy balance components for all six sites. R_n exhibits a symmetric bell shape distribution with daytime maximum around local noon. Across all sites, H and LE attain their maximum values around local noon and decline towards nighttime, closely tracking the diurnal course of R_n. The ground heat flux (G) exhibits an inverse phase relative to H and LE, with predominantly negative values during daytime and positive values during nighttime. Note that the dataset adheres to the convention in which positive fluxes denote transport away from the surface and negative fluxes denote transport towards the surface. Consequently, the sign of G has been inverted here solely for visualization purposes. Site-specific differences in R_n and its partitioning in H, LE and G are evident, and reflect previously discussed variations in vegetation structure, surface roughness and measurement configuration. With respect to variations in R_n, a distinct gradient is apparent, extending from the forest sites through the cropland sites to the degraded grassland sites. This gradient is consistent with previously reported differences in surface albedo and vegetation

https://doi.org/10.5194/essd-2026-379
Preprint. Discussion started: 22 July 2026

structure across the same land use types (Hingerl et al., 2025). Forest sites exhibit the highest daytime R_n due to lower albedo as a result of a denser vegetation cover, degraded and semi-degraded grassland sites show systematically reduced R_n associated with sparse vegetation and a brighter soil surface. Cropland and rainfed rice field sites occupy an intermediate position along the gradient, as their vegetation cover during the plantation period is high compared to the degraded grassland. The agreement between the climatological diurnal cycles shown here and the land use dependent site characteristics reported in Hingerl et al. (2025) as well as the overall similarity of their diurnal dynamics further supports the physical consistency and representativeness of the energy flux measurements across all sites.

5 Usage notes

The dataset is suitable for a wide range of applications, including land surface and Earth system model evaluation, studies of land-atmosphere coupling, and comparative analyses across land use and management gradients. In addition, the data can be used for the validation of satellite- and machine-learning-based products of evapotranspiration and carbon fluxes, as well as for analyses of seasonal to interannual variability and ecosystem responses to hydroclimatic extremes. To facilitate appropriate use and interpretation of the dataset, the following usage notes and recommendations are provided:

- Users are advised to apply quality filtering based on the provided EddyPro quality flags. For most applications, data with QC ≤ 1 are recommended, while analyses focusing on short-term processes or event-scale dynamics may preferentially rely on data with QC = 0.
- Nighttime CO_2 fluxes should be interpreted with caution under stable atmospheric conditions, as low turbulence can lead to an underestimation of ecosystem respiration. Users may therefore consider additional filtering based on friction velocity (u_*) thresholds or atmospheric stability metrics, depending on the specific research objective.
- Energy flux analyses should account for the fact that no energy balance closure correction has been applied. Deviations from closure are consistent with site-specific characteristics and should be considered when interpreting surface energy partitioning rather than being treated as measurement errors.
- No gap filling has been applied; missing values are explicitly retained to allow flexible user-defined gap-filling approaches. The predominance of short data gaps provides favorable conditions for the application of established gap-filling techniques.
- For sites characterized by heterogeneous surface conditions, particularly Mole and Gorigo, users are encouraged to consider the provided footprint information when conducting spatially explicit analyses or comparisons with satellite-based products.

https://doi.org/10.5194/essd-2026-379
Preprint. Discussion started: 22 July 2026

6 Data availability

The dataset presented in this paper is publicly available through the PANGAEA Data Publisher for Earth & Environmental Science under https://doi.org/10.1594/PANGAEA.994143.

Hingerl, L., Guug, S., Bliefernicht, J., Kadum, H., Sy, S., Sawadogo, W., Quansah, E., Oussou, F.E., Amekudzi, L., Salack, S., Diallo, B.A.-A. Ayamba, M., Ramde, E., Steinbrecher, R., Neidl, F., Kunstmann, H., *Long-term eddy-covariance measurements of energy, water, and carbon fluxes across a savanna land-use gradient in West Africa* [dataset publication series]. PANGAEA, https://doi.org/10.1594/PANGAEA.994143, 2026.

The dataset includes harmonized half-hourly and daily observations of carbon, water, and energy fluxes, meteorological variables, and ancillary measurements from six savanna ecosystems in Burkina Faso and Ghana. All data files, metadata, quality flags, and documentation required for data reuse are provided through the PANGAEA repository. At the time of manuscript submission, the dataset has been archived in PANGAEA and assigned the DOI given above.

7 Conclusions

We present a harmonized, multisite eddy-covariance dataset for the West African Sudanian Savanna covering the period from 2013 to 2025, comprising six stations distributed along a land use gradient that includes near-natural vegetation, cropland, and degraded grassland. The distinctive scientific value of this data set resides in its combination of long-term reference sites (Nazinga, Kayoro, Sumbrungu/Gorigo) with instrumentally enhanced monitoring sites (Janga, Mole). This design enables robust analysis of temporal variability over extended periods, while simultaneously allowing for the quantification of current management effects. The dataset was processed using a standardized workflow (EddyPro followed by subsequent post-processing), adhering to FLUXNET-compliant variable nomenclature and unit conventions, applying uniform sign conventions, and aggregating all variables at a consistent temporal resolution of 30 minutes. All quality control (QC) flags have been fully preserved, allowing users to select an appropriate filtering strategy tailored to their specific use case. In addition, plausibility limits were applied to identify and remove non-physical values. The heatmap representation of data coverage indicates generally high coverage for the central flux variables. Gap statistics demonstrate a high degree of temporal continuity, with a median gap length of 0.5 hours. Longer gaps occur less frequently and can be attributed to scheduled maintenance, technical malfunctions, and data filtering procedures. A technical validation was conducted to confirm the internal consistency of the data set by demonstrating physically coherent patterns in energy and CO_2 fluxes. These include, for example, realistic diurnal dynamics of the individual energy flux components, as well as plausible responses of evapotranspiration and soil moisture to precipitation events. The analysis of turbulence and stability fingerprints, as well as the footprints of turbulent fluxes, indicates that land use type, surface heterogeneity, and measurement configuration (e.g. measurement height) systematically affect the turbulence regime and, consequently, the interpretability of the turbulent fluxes, particularly nighttime CO_2 fluxes. The data set is intended, for example, for use in the following application scenarios:

– Evaluation and benchmarking of land surface models and Earth system models, as well as reanalysis products (Poan et al., 2016; Foli et al., 2022; Fischer et al., 2025).

– Investigations of land–atmosphere coupling processes and feedbacks in semi-arid savanna ecosystems (Müller et al., 2021; Talib et al., 2022).

– Comparative analyses across land use and land-management gradients, including near-natural, cropland, and degraded savanna systems (Mamadou et al., 2016, 2025; Sy and Quesada, 2020; Nadolski et al., 2024; Hingerl et al., 2025; Guug et al., 2025).

– Validation and development of satellite- and machine-learning-based products of evapotranspiration, net ecosystem exchange (NEE/NEP), and surface energy partitioning (Weerasinghe et al., 2020; Nelson et al., 2024; El Hachimi et al., 2024).

– Analyses of interannual variability, seasonal memory effects, and ecosystem responses to hydroclimatic extremes such as droughts and anomalous rainfall events (Lohou et al., 2014; Berger et al., 2019; Bliefernicht et al., 2022; Rigatti et al., 2024).

Overall, the presented dataset constitutes a robust and extensible observational basis capable of supporting future expansions of the monitoring network, as well as the incorporation of additional variables that are not currently included in the released data product. Such extensions, encompassing, for example, longer-term trace gas observations and enhanced process-level budget analyses via the inclusion of storage and advection terms, can be implemented without compromising either the internal consistency or the immediate practical usability of the existing dataset.

Appendix A: Data records

A1 Repository structure and file naming

The processed dataset is archived in the PANGAEA data repository and consists of harmonized eddy-covariance flux and meteorological time series for the six measurement sites, together with accompanying metadata tables. All data are provided in tab-separated values (TSV) format with UTF-8 encoding.

A1.1 File structure

The archive comprises 12 station-specific time-series files and three metadata files that document the measurement campaign, individual sites (events), and observed parameters.

For each measurement site, two time-series datasets are provided:

– a **half-hourly TSV dataset** containing processed eddy-covariance fluxes and meteorological variables at 30 min temporal resolution,

https://doi.org/10.5194/essd-2026-379
Preprint. Discussion started: 22 July 2026

Open Access Earth System Science Data Discussions

– a **daily TSV dataset** containing aggregated daily averages or sums derived from the half-hourly data,

In addition, three repository-wide metadata files describe the overall campaign, the characteristics of each measurement site, and the variables contained in the time-series files:

– **campaign_metadata.tsv** — campaign-level information (label, basis, temporal coverage, responsible scientists, and general description),

– **event_metadata.tsv** — site-level information for each measurement location (coordinates, elevation, operational period, instrumentation, land use, and site description), and

– **parameter_metadata.tsv** — variable definitions (short names, full names, units, principal investigator, and instrument or processing method).

The files included in the dataset are listed in Tables A1 and A2.

Table A1. Overview of provided time-series data files in TSV format for all measurement sites, separated by temporal resolution.

Station	30 min data	Daily data
Gorigo	Gorigo_30min.tsv	Gorigo_daily.tsv
Kayoro	Kayoro_30min.tsv	Kayoro_daily.tsv
Nazinga	Nazinga_30min.tsv	Nazinga_daily.tsv
Janga	Janga_30min.tsv	Janga_daily.tsv
Mole	Mole_30min.tsv	Mole_daily.tsv
Sumbrungu	Sumbrungu_30min.tsv	Sumbrungu_daily.tsv

Table A2. Metadata files describing the measurement campaign, individual sites, and observed parameters.

File	Scope	Contents
campaign_metadata.tsv	Campaign	Campaign label, basis, start and end date/time (UTC), responsible scientists, description
event_metadata.tsv	Site/event	Event label, coordinates, elevation, operational period, instrumentation, campaign link, land use, description
parameter_metadata.tsv	Variables	Short name, full name, unit, principal investigator, instrument or method

A1.2 File naming convention

Time-series files follow the standardized naming scheme

```
[SiteName]_[temporal_resolution].[file_format]
```

https://doi.org/10.5194/essd-2026-379
Preprint. Discussion started: 22 July 2026

where

- **SiteName** identifies the measurement site (Nazinga, Kayoro, Sumbrungu, Gorigo, Janga, or Mole),
- **temporal_resolution** specifies the temporal aggregation level of the data (30min or daily), and
- **file_format** indicates the file type (tsv).

Metadata files follow a fixed, descriptive naming scheme:

`[campaign|event|parameter]_metadata.[file_format]`

where **campaign**, **event**, or **parameter** indicates the metadata level and **file_format** is tsv.

A1.3 File format and data structure

All TSV files use tab characters as field delimiters and contain a single header row with column names, followed by the data records. Missing or unavailable values are encoded as `-9999`.

A1.4 Time-series files.

Each time-series file begins with three leading columns that identify the measurement site, its elevation, and the observation time:

- **Event** — site name (Gorigo, Janga, Kayoro, Mole, Nazinga, or Sumbrungu), consistent with the `Event_Label` field in `event_metadata.tsv`,
- **Elevation [m a.s.l.]** — station elevation above sea level in metres, and
- **Date/Time [UTC]** — timestamp in ISO 8601 format (`YYYY-MM-DDTHH:MM:SS`), representing the start of the averaging period in UTC for both temporal resolutions.

All subsequent columns contain measured or derived variables. Variable names follow the PANGAEA convention of combining the full parameter name with the physical unit in square brackets, for example `Latent heat flux [W m-2]` and `Air temperature [degC]`. Definitions, units, and provenance of these variables are documented in `parameter_metadata.tsv`, which links short internal identifiers such as `LE` and `NEE` to the full column names used in the time-series files.

The half-hourly datasets contain the full set of processed eddy-covariance fluxes, radiation components, meteorological variables, turbulence parameters, and soil measurements, including associated quality flags for turbulent fluxes and net ecosystem exchange. The daily datasets contain aggregated daily values derived from the half-hourly observations; quality-flag columns are not included at daily resolution.

A1.5 Metadata files.

The three metadata files use the same TSV structure (single header row, one record per campaign, site, or parameter, respectively) and complement the time-series files as follows:

- **campaign_metadata.tsv** contains one row describing the WASCAL Eddy Covariance Observatory campaign, including the campaign label, observational basis, overall start and end date/time in UTC, responsible scientists, and a general description of the network.
- **event_metadata.tsv** contains one row per measurement site (Gorigo, Janga, Kayoro, Mole, Nazinga, and Sumbrungu), documenting geographic coordinates (WGS84), elevation, site-specific operational period, instrumentation, associated campaign, land-use class, and a textual site description. The `Event_Label` field corresponds to the `Event` column in the time-series files.
- **parameter_metadata.tsv** contains one row per variable, providing the short parameter identifier, full parameter name, unit, principal investigator, and instrument or processing method. This file serves as the authoritative reference for interpreting the parameter columns in the time-series files.

A1.6 Variable naming conventions

Variable names follow the requirements of the PANGAEA data repository, where each column header contains the full parameter name together with its unit in square brackets. This ensures that the data tables are self-describing and directly interpretable without the need for external metadata.

The dataset includes turbulent fluxes (e.g. latent and sensible heat flux, net ecosystem CO_2 exchange, and momentum flux) together with their associated quality flags following the Spoleto convention (0 = high, 1 = moderate, 2 = low quality). Additional variables describe radiation components (incoming and outgoing shortwave and longwave radiation, net radiation), meteorological conditions (air temperature, relative humidity, vapour pressure deficit, atmospheric pressure, wind speed, and wind direction), turbulence parameters (friction velocity, stability parameter z/L, and Monin–Obukhov length), as well as water balance variables (precipitation and evapotranspiration). Soil measurements include soil heat flux, soil temperature, and volumetric soil water content at multiple depths. In addition to the general quality flags, a site-specific quality flag is provided for the Kayoro station to indicate potential footprint disturbances caused by a nearby school building. Observations with wind directions between 196° and 228° from October 2016 onwards are flagged as potentially affected (value = 1), while all other observations are marked as unaffected (value = 0). All variables are provided at a temporal resolution of 30 min, with daily aggregated values derived accordingly. Table 4 provides a complete overview of all variables, including their full column headers and additional information.

https://doi.org/10.5194/essd-2026-379
Preprint. Discussion started: 22 July 2026

Open Access Earth System Science Data Discussions

Appendix B: Gap length distribution

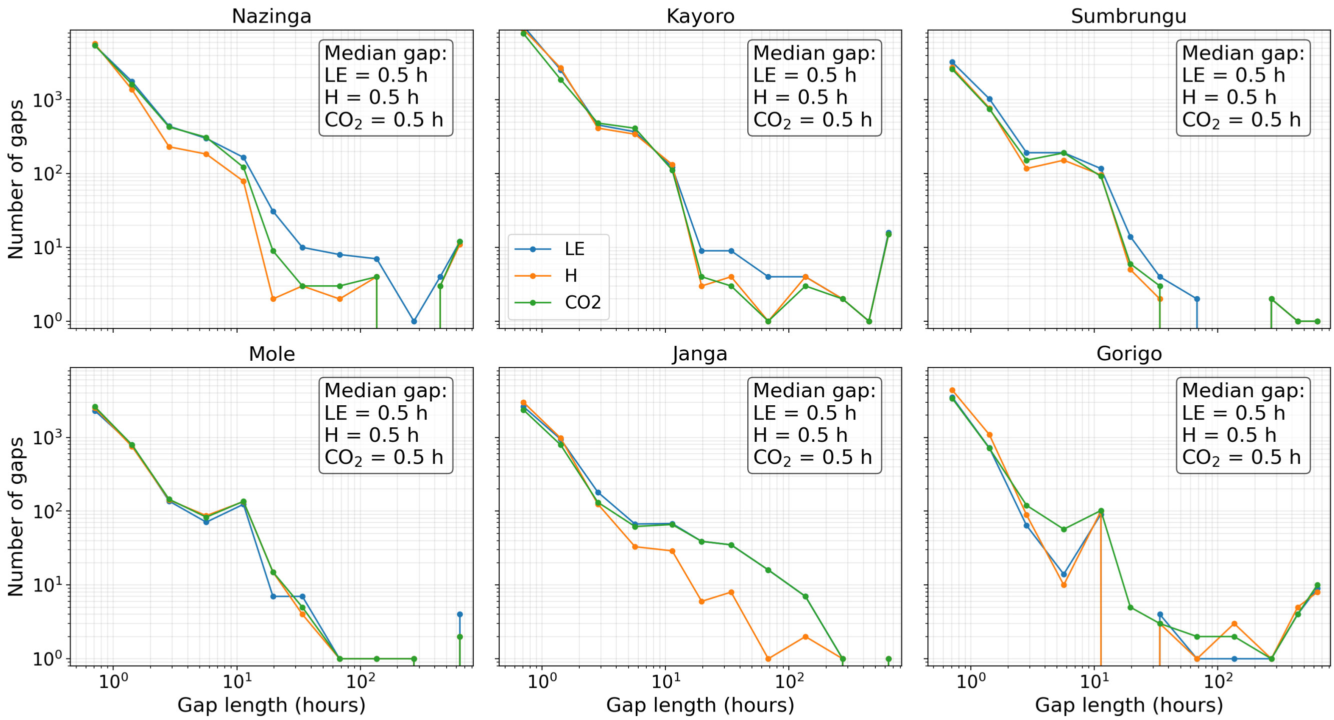

Figure B1. Gap-length distributions of half hourly LE, H and CO_2 time series for all six eddy-covariance stations after quality filtering ($QC \leq 1$). Shown are the frequencies of consecutive data gaps on the 30 min time grid, expressed as a function of gap length in hours. Gap statistics were computed over the same station-specific time periods as illustrated in the monthly data availability heat map (Fig. 2), ensuring consistency between coverage metrics and gap-length diagnostics. The dominance of short gaps indicates high temporal continuity of the data sets, while longer gaps occur less frequently and are site- and variable-specific.

https://doi.org/10.5194/essd-2026-379
Preprint. Discussion started: 22 July 2026

Open Access Earth System Science Data Discussions

600 ## Appendix C: Mean diurnal cycle of CO_2 exchange

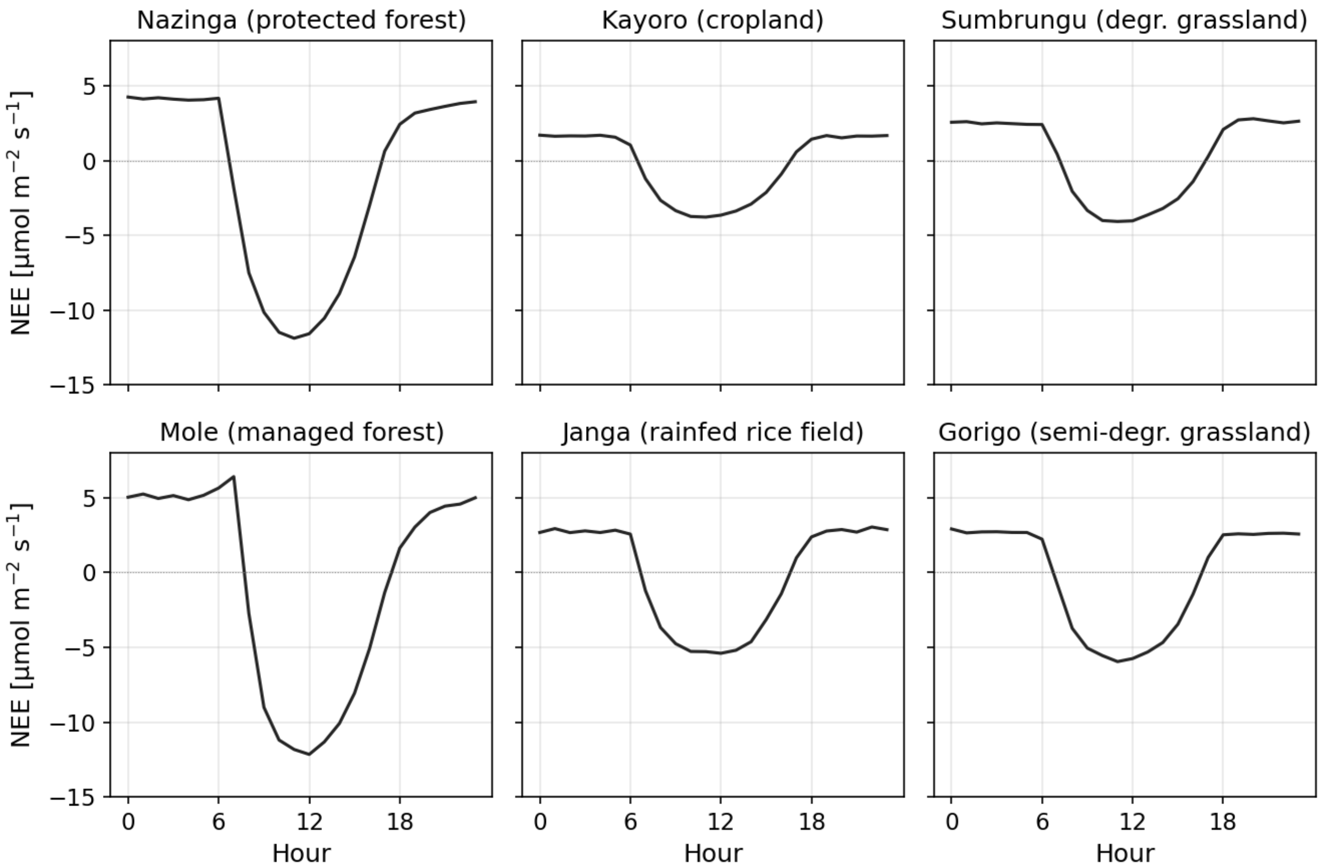

Figure C1. Mean diurnal cycle of ecosystem–atmosphere CO_2 exchange at the six study sites derived from quality controlled eddy-covariance measurements (QC $\leq$ 1). Shown are multi-year mean half-hourly turbulent CO_2 fluxes averaged by hour of day over all available years. Negative values indicate net ecosystem CO_2 uptake, whereas positive values indicate net CO_2 release to the atmosphere. All sites exhibit the characteristic diurnal cycle of terrestrial ecosystems, with positive fluxes during nighttime caused by ecosystem respiration and negative fluxes during daytime due to photosynthetic CO_2 uptake. The near-natural savanna sites Nazinga and Mole show the strongest daytime uptake and the largest diurnal amplitude, whereas the cropland and degraded grassland sites exhibit weaker daytime CO_2 uptake. The timing and magnitude of the minimum flux around midday further illustrate site specific differences in vegetation activity and ecosystem functioning.

Author contributions. Luitpold Hingerl designed the study, compiled and harmonized the multi-site dataset, performed the analyses, prepared the figures, wrote the original manuscript draft, and contributed to the installation and maintenance of several measurement stations.

https://doi.org/10.5194/essd-2026-379
Preprint. Discussion started: 22 July 2026

Samuel Guug and Rainer Steinbrecher contributed to the installation and maintenance of several stations. Samuel Guug also provided data and contributed substantially to the interpretation of the results and revision of the manuscript. Frank Neidl provided IT support for data acquisition, processing, and management. Jan Bliefernicht, Hawwa Kadum, and Souleymane Sy contributed to the interpretation of the results and provided substantial revisions to the manuscript. Windmanagda Sawadogo and Emmanuel Quansah reviewed the manuscript and provided comments. Harald Kunstmann supervised the study and contributed to the conceptual development and revision of the manuscript. All authors read and approved the final manuscript.

Competing interests. The authors declare that they have no competing interests.

Acknowledgements. This research was funded by the German Federal Ministry of Education and Research (BMBF) through the West African Science Service Center on Climate Change and Adapted Land Use and the Concerted Regional Modelling and Observation Assessment for Greenhouse Gas Emissions and Mitigation Options under Climate and Land Use Change in West Africa (CONCERT-West Africa; Grant No. 01LG2089A BMBF). The authors gratefully acknowledge the authorities of Mole National Park and the Forestry Commission for permitting the installation and operation of the eddy covariance station in Mole. We further thank Chief Ibrahim Johnson, landlord of the Janga rice field, for granting access and permission to establish the eddy covariance station at Janga. We are also grateful to all technicians, field assistants, and local collaborators who supported the installation, maintenance, and long-term operation of the stations.

https://doi.org/10.5194/essd-2026-379
Preprint. Discussion started: 22 July 2026

Open Access Earth System Science Data Discussions

References

Abdaki, M., Sanchez-Azofeifa, A., and Hamann, H. F.: A machine learning approach for filling long gaps in eddy covariance time series data in a tropical dry forest, Journal of Geophysical Research: Biogeosciences, 130, e2024JG008 375, 2025.

Ago, E. E., Agbossou, E. K., Galle, S., Cohard, J.-M., Heinesch, B., and Aubinet, M.: Long term observations of carbon dioxide exchange over cultivated savanna under a Sudanian climate in Benin (West Africa), Agricultural and Forest Meteorology, 197, 13–25, 2014.

Ago, E. E., Serça, D., Agbossou, E. K., Galle, S., and Aubinet, M.: Carbon dioxide fluxes from a degraded woodland in West Africa and their responses to main environmental factors, Carbon balance and management, 10, 22, 2015.

Ago, E. E., Agbossou, E. K., Cohard, J.-M., Galle, S., and Aubinet, M.: Response of CO2 fluxes and productivity to water availability in two contrasting ecosystems in northern Benin (West Africa), Annals of Forest Science, 73, 483–500, 2016.

Aryee, J., Amekudzi, L., Preko, K., Atiah, W., and Danuor, S.: Estimation of planetary boundary layer height from radiosonde profiles over West Africa during the AMMA field campaign: Intercomparison of different methods, Scientific African, 7, e00 228, 2020.

Bagayoko, F., Yonkeu, S., and Van de Giesen, N.: Energy balance closure and footprint analysis using Eddy Covariance measurements in Eastern Burkina Faso, West Africa, Hydrology and Earth System Sciences Discussions, 3, 2789–2812, 2006.

Berger, S., Bliefernicht, J., Linstädter, A., Čanak, K., Guug, S., Heinzeller, D., Hingerl, L., Mauder, M., Neidl, F., Quansah, E., Salack, S., Steinbrecher, R., and Kunstmann, H.: The impact of rain events on CO2 emissions from contrasting land use systems in semi-arid West African savannas, Science of The Total Environment, 647, 1478–1489, https://doi.org/https://doi.org/10.1016/j.scitotenv.2018.07.397, 2019.

Bliefernicht, J., Kunstmann, H., Hingerl, L., Rummler, T., Andresen, S., Mauder, M., Steinbrecher, R., Friess, R., Gochis, D., Gessner, U., et al.: Field-and Simulation Experiments for the Investigating regional Land-Atmosphere Interactions within the West Africa: experimental set-up and first results, IAHS Publ. 359, 2013, pp. 226–232, 2013.

Bliefernicht, J., Berger, S., Salack, S., Guug, S., Hingerl, L., Heinzeller, D., Mauder, M., Steinbrecher, R., Steup, G., and Bossa, A. Y.: The WASCAL hydrometeorological observatory in the Sudan Savanna of Burkina Faso and Ghana, Vadose Zone Journal, 17, 1–20, 2018.

Bliefernicht, J., Salack, S., Waongo, M., Annor, T., Laux, P., and Kunstmann, H.: Towards a historical precipitation database for West Africa: Overview, quality control and harmonization, 2022.

Blonquist Jr, J., Tanner, B., and Bugbee, B.: Evaluation of measurement accuracy and comparison of two new and three traditional net radiometers, Agricultural and Forest Meteorology, 149, 1709–1721, 2009.

Boone, A. A., Xue, Y., Sales, F. D., Comer, R. E., Hagos, S., Mahanama, S., Schiro, K., Song, G., Wang, G., and Li, S.: The regional impact of Land-Use Land-cover Change (LULCC) over West Africa from an ensemble of global climate models under the auspices of the WAMME2 project, Climate Dynamics, 47, 3547–3573, 2016.

Brümmer, C., Falk, U., Papen, H., Szarzynski, J., Wassmann, R., and Brüggemann, N.: Diurnal, seasonal, and interannual variation in carbon dioxide and energy exchange in shrub savanna in Burkina Faso (West Africa), Journal of Geophysical Research: Biogeosciences, 113, 2008.

Butterworth, B. J., Desai, A. R., Durden, D., Kadum, H., LaLuzerne, D., Mauder, M., Metzger, S., Paleri, S., and Wanner, L.: Characterizing energy balance closure over a heterogeneous ecosystem using multi-tower eddy covariance, Frontiers in Earth Science, 11, 1251 138, 2024.

Ceperley, N. C., Mande, T., Van De Giesen, N., Tyler, S., Yacouba, H., and Parlange, M. B.: Evaporation from cultivated and semi-wild Sudanian Savanna in west Africa, Hydrology and Earth System Sciences, 21, 4149–4167, 2017.

https://doi.org/10.5194/essd-2026-379
Preprint. Discussion started: 22 July 2026

Copernicus Climate Change Service: Land Cover Maps - v2.1.1 (1992–2022), https://doi.org/10.24381/cds.006f2c9a, 2023.

El Hachimi, C., Khabba, S., Belaqziz, S., Hssaine, B. A., Kharrou, M. H., and Chehbouni, A.: Are raw satellite bands and machine learning all you need to retrieve actual evapotranspiration?, in: E3S Web of Conferences, vol. 489, p. 04019, EDP Sciences, 2024.

Fischer, M., Knippertz, P., and Proppe, C.: Surrogate-based model parameter optimization in simulations of the West African monsoon, Weather and Climate Dynamics, 6, 113–130, 2025.

Flörke, M., Schneider, C., and McDonald, R. I.: Water competition between cities and agriculture driven by climate change and urban growth, Nature Sustainability, 1, 51–58, 2018.

Foken, T. and Wichura, B.: Tools for quality assessment of surface-based flux measurements, Agricultural and forest meteorology, 78, 83–105, 1996.

Foli, B. A. K., Appeaning Addo, K., Ansong, J. K., and Wiafe, G.: Evaluation of ECMWF and NCEP reanalysis wind fields for long-term historical analysis and ocean wave modelling in West Africa, Remote Sensing in Earth Systems Sciences, 5, 26–45, 2022.

Galle, S., Grippa, M., Peugeot, C., Moussa, I. B., Cappelaere, B., Demarty, J., Mougin, E., Panthou, G., Adjomayi, P., Agbossou, E., et al.: AMMA-CATCH, a critical zone observatory in West Africa monitoring a region in transition, Vadose Zone Journal, 17, 1–24, 2018.

Gao, D., Yao, J., Yu, S., Ma, Y., Li, L., and Gao, Z.: Eddy covariance CO2 flux gap filling for long data gaps: A novel framework based on machine learning and time series decomposition, Remote Sensing, 15, 2695, 2023.

Guug, S., Sy, S., Quansah, E., Bliefernicht, J., Neidl, F., Steinbrecher, R., Ayamba, M., Frempong, A., Davies, P., Spangenberg, I., et al.: Methane emissions from rice cultivation in West Africa and compensation options from nature reserve forests, Environmental Research Letters, 20, 044 050, 2025.

Hingerl, L., Bliefernicht, J., Guug, S., Sy, S., Neidl, F., Jagdhuber, T., and Kunstmann, H.: Comparative analysis of land–atmosphere interactions across three contrasting ecosystems in the West Sudanian Savanna, Journal of Hydrology: Regional Studies, 61, 102 751, 2025.

Hutley, L. B., Leuning, R., Beringer, J., and Cleugh, H. A.: The utility of the eddy covariance techniques as a tool in carbon accounting: tropical savanna as a case study, Australian Journal of Botany, 53, 663–675, 2005.

Jentzsch, K., Boike, J., and Foken, T.: Importance of the Webb, Pearman, and Leuning (WPL) correction for the measurement of small CO 2 fluxes, Atmospheric Measurement Techniques, 14, 7291–7296, 2021.

Kaimal, J. C. and Finnigan, J. J.: Atmospheric boundary layer flows: their structure and measurement, Oxford university press, 1994.

Kormann, R. and Meixner, F. X.: An analytical footprint model for non-neutral stratification, Boundary-Layer Meteorology, 99, 207–224, 2001.

Koster, R. D., Dirmeyer, P. A., Guo, Z., Bonan, G., Chan, E., Cox, P., Gordon, C., Kanae, S., Kowalczyk, E., Lawrence, D., et al.: Regions of strong coupling between soil moisture and precipitation, Science, 305, 1138–1140, 2004.

Koster, R. D., Sud, Y. C., Guo, Z., Dirmeyer, P. A., Bonan, G., Oleson, K. W., Chan, E., Verseghy, D., Cox, P., and Davies, H.: GLACE: the global land-atmosphere coupling experiment. Part I: overview, Journal of Hydrometeorology, 7, 590–610, 2006.

Koukoui, R., Mamadou, O., Houénou, F., Heinesch, B., Bousso, M., and Cohard, J.-M.: Ten years of carbon dioxide fluxes and carbon balance at a mixed cultivated savannah and an open forest in a tropical humid climate in West Africa, in: EGU General Assembly Conference Abstracts, pp. EGU25–16 269, 2025.

Lebel, T., Cappelaere, B., Galle, S., Hanan, N., Kergoat, L., Levis, S., Vieux, B., Descroix, L., Gosset, M., Mougin, E., et al.: AMMA-CATCH studies in the Sahelian region of West-Africa: An overview, Journal of Hydrology, 375, 3–13, 2009.

LI-COR Biosciences: Eddy Covariance Processing Software (EddyPro®) Version 7.0.8, https://www.licor.com/EddyPro, software, 2021.

Liebethal, C. and Foken, T.: On the significance of the Webb correction to fluxes, Boundary-Layer Meteorology, 109, 99–106, 2003.

https://doi.org/10.5194/essd-2026-379
Preprint. Discussion started: 22 July 2026

Lohou, F., Kergoat, L., Guichard, F., Boone, A., Cappelaere, B., Cohard, J.-M., Demarty, J., Galle, S., Grippa, M., Peugeot, C., et al.: Surface response to rain events throughout the West African monsoon, Atmospheric Chemistry and Physics, 14, 3883–3898, 2014.

Mamadou, O., Galle, S., Cohard, J.-M., Peugeot, C., Kounouhewa, B., Biron, R., Hector, B., and Zannou, A. B.: Dynamics of water vapor and energy exchanges above two contrasting Sudanian climate ecosystems in Northern Benin (West Africa), Journal of Geophysical Research: Atmospheres, 121, 11–269, 2016.

Mamadou, O., Cohard, J.-M., Hounsinou, M., Koukoui, R., Afouda, S., Barral, H., Biron, R., Cuvelier, L., Mariscal, A., Ouani, T., et al.: Land use change impacts on H2O and CO2 surface/atmosphere fluxes derived from two Eddy-Covariance stations under sudanian climate in West Africa, in: ARPHA Conference Abstracts, vol. 8, p. e151363, Pensoft Publishers, 2025.

Mauder, M., Cuntz, M., Drüe, C., Graf, A., Rebmann, C., Schmid, H. P., Schmidt, M., and Steinbrecher, R.: A strategy for quality and uncertainty assessment of long-term eddy-covariance measurements, Agricultural and Forest Meteorology, 169, 122–135, 2013.

Mauder, M., Jung, M., Stoy, P., Nelson, J., and Wanner, L.: Energy balance closure at FLUXNET sites revisited, Agricultural and Forest Meteorology, 358, 110 235, 2024.

Moore, C.: Frequency response corrections for eddy correlation systems, Boundary-Layer Meteorology, 37, 17–35, 1986.

Mortey, E. M., Annor, T., Arnault, J., Inoussa, M. M., Madougou, S., Kunstmann, H., and Nyantakyi, E. K.: Interactions between Climate and Land Cover Change over West Africa, Land, 12, 355–355, https://doi.org/https://doi.org/10.3390/land12020355, 2023.

Müller, O. V., Vidale, P. L., Vannière, B., Schiemann, R., Senan, R., Haarsma, R. J., and Jungclaus, J. H.: Land–atmosphere coupling sensitivity to GCMs resolution: A multimodel assessment of local and remote processes in the Sahel hot spot, Journal of Climate, 34, 967–985, 2021.

Nadolski, L., Bliefernicht, J., Petrovic, D., Rauch, M., Sy, S., Guug, S., Steinbrecher, R., Neidl, F., Hingerl, L., and Kunstmann, H.: Exploring and closing the energy balance of eddy covariance measurements along a land use gradient in the West African Sudanian savanna, Frontiers in Water, https://doi.org/10.3389/frwa.2024.1393884, 2024.

Nelson, J. A., Walther, S., Gans, F., Kraft, B., Weber, U., Novick, K., Buchmann, N., Migliavacca, M., Wohlfahrt, G., Šigut, L., et al.: X-BASE: the first terrestrial carbon and water flux products from an extended data-driven scaling framework, FLUXCOM-X, Biogeosciences, 21, 5079–5115, 2024.

Neupane, R. P. and Kumar, S.: Estimating the effects of potential climate and land use changes on hydrologic processes of a large agriculture dominated watershed, Journal of Hydrology, 529, 418–429, 2015.

Poan, E. D., Gachon, P., Dueymes, G., Diaconescu, E., Laprise, R., and Seidou Sanda, I.: West African monsoon intraseasonal activity and its daily precipitation indices in regional climate models: diagnostics and challenges, Climate Dynamics, 47, 3113–3140, 2016.

Potapov, P., Turubanova, S., Hansen, M. C., Tyukavina, A., Zalles, V., Khan, A., Song, X.-P., Pickens, A., Shen, Q., and Cortez, J.: Global maps of cropland extent and change show accelerated cropland expansion in the twenty-first century, Nature Food, 3, 19–28, 2022.

Quansah, E., Mauder, M., Balogun, A. A., Amekudzi, L. K., Hingerl, L., Bliefernicht, J., and Kunstmann, H.: Carbon dioxide fluxes from contrasting ecosystems in the Sudanian Savanna in West Africa, Carbon balance and management, 10, 1–17, 2015.

Rigatti, E., McDermid, S. S., Cook, B. I., and De Kauwe, M. G.: The impact of drought on terrestrial carbon in the West African Sahel: Implications for natural climate solutions, Journal of Geophysical Research: Biogeosciences, 129, e2024JG008 143, 2024.

Schotanus, P., Nieuwstadt, F., and De Bruin, H.: Temperature measurement with a sonic anemometer and its application to heat and moisture fluxes, Boundary-Layer Meteorology, 26, 81–93, 1983.

Snyder, P. K., Delire, C., and Foley, J. A.: Evaluating the influence of different vegetation biomes on the global climate, Climate Dynamics, 23, 279–302, 2004.

https://doi.org/10.5194/essd-2026-379
Preprint. Discussion started: 22 July 2026

Sy, S. and Quesada, B.: Anthropogenic land cover change impact on climate extremes during the 21st century, Environmental Research Letters, 15, 034 002, https://doi.org/10.1088/1748-9326/ab702c, 2020.

Sy, S., de Noblet-Ducoudré, N., Quesada, B., Sy, I., Dieye, A. M., Gaye, A. T., and Sultan, B.: Land-surface characteristics and climate in West Africa: Models' biases and impacts of historical anthropogenically-induced deforestation, Sustainability, 9, 1917, 2017.

Sy, S., Bliefernicht, J., Manevski, K., Guug, S., Hingerl, L., Quesada, B., Oussou, F. E., Kiese, R., Davies, P., Jagdhuber, T., et al.: Water use efficiency responses in contrasting agroecosystems and land management practices in West Africa, 2026.

Talib, J., Taylor, C. M., Klein, C., Harris, B. L., Anderson, S. R., and Semeena, V. S.: The sensitivity of the West African monsoon circulation to intraseasonal soil moisture feedbacks, Quarterly Journal of the Royal Meteorological Society, 148, 1709–1730, 2022.

Verhoef, A., Allen, S. J., De Bruin, H. A., Jacobs, C. M., and Heusinkveld, B. G.: Fluxes of carbon dioxide and water vapour from a Sahelian savanna, Agricultural and Forest Meteorology, 80, 231–248, 1996.

Vickers, D. and Mahrt, L.: Quality control and flux sampling problems for tower and aircraft data, Journal of Atmospheric and Oceanic Technology, 1997.

Waller, M. P., Street-Perrott, F. A., and Wang, H.: Holocene vegetation history of the Sahel: pollen, sedimentological and geochemical data from Jikariya Lake, north-eastern Nigeria, Journal of Biogeography, 34, 1575–1590, 2007.

Wanner, L., Jung, M., Paleri, S., Butterworth, B. J., Desai, A. R., Sühring, M., and Mauder, M.: Towards energy-balance closure with a model of dispersive heat fluxes, Boundary-Layer Meteorology, 190, 25, 2024.

Webb, E. K., Pearman, G. I., and Leuning, R.: Correction of flux measurements for density effects due to heat and water vapour transfer, Quarterly Journal of the Royal Meteorological Society, 1980.

Weerasinghe, I., Bastiaanssen, W., Mul, M., Jia, L., and Van Griensven, A.: Can we trust remote sensing evapotranspiration products over Africa?, Hydrology and Earth System Sciences, 24, 1565–1586, 2020.

Wieckowski, A., Vestin, P., Ardö, J., Roupsard, O., Ndiaye, O., Diatta, O., Ba, S., Agbohessou, Y., Fensholt, R., Verbruggen, W., et al.: Eddy covariance measurements reveal a decreased carbon sequestration strength 2010–2022 in an African semiarid savanna, Global Change Biology, 30, e17 509, 2024.

Xue, Y.: Impact of Land–Atmosphere Interactions on Sahel Climate, Oxford Research Encyclopedia of Climate Science, https://doi.org/https://doi.org/10.1093/acrefore/9780190228620.013.514, 2017.

Yu, R., Ruddell, B. L., Kang, M., Kim, J., and Childers, D.: Anticipating global terrestrial ecosystem state change using FLUXNET, Global change biology, 25, 2352–2367, 2019.